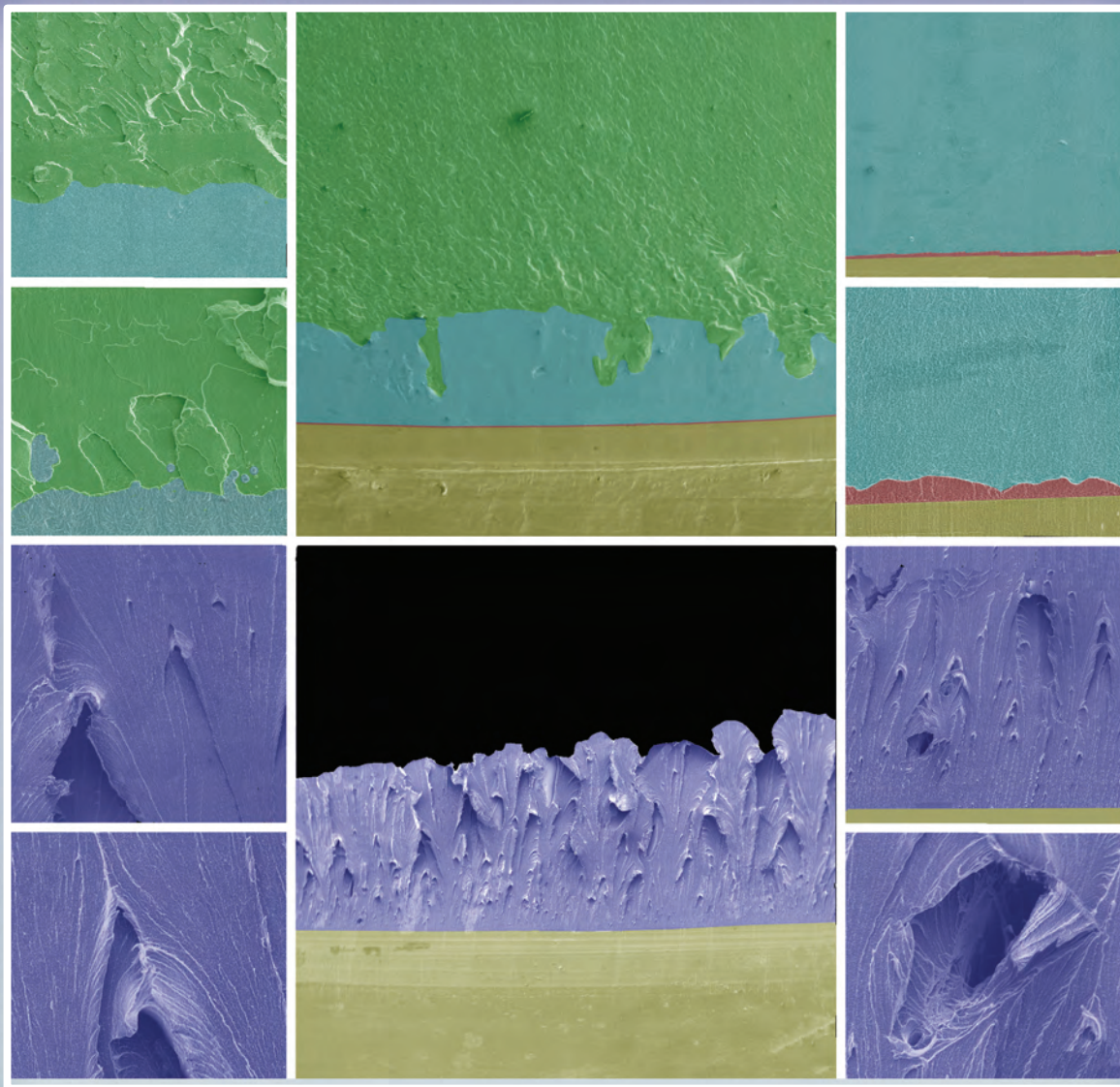


nuclear weapons journal



Issue 2 2006

- Fracture and Damage Evolution in Polymers ■
- Validating ASC Codes ■ Gated X-Ray Detector for the NIF ■
- UNICORN Yields Crucial Data ■

Contents

Fracture and Damage Evolution
in Polymers 1

Using Double-Shell Target Experiments
to Validate ASC Codes 8

Gated X-Ray Detector for the NIF 15

UNICORN Experiments Yield
Crucial Data 20

PTLA: Ensuring Safety
through Training 22

Waste Reduction at the Laboratory 25

Violence in the Workplace 28

Safety at LANL: the New Paradigm 30

About the cover: These scanning electron microscopy images of the polymer Kel-F 800, used as the binder in plastic-bonded explosives, are colored to highlight fracture surfaces at different temperatures and levels of magnification. LANL's research on fracture origin and development in polymers has the potential for significant impacts on industry, defense, and surgical medicine.

Issue 2, 2006 LALP-06-084

Nuclear Weapons Journal highlights ongoing work in the nuclear weapons program at Los Alamos National Laboratory. *NWJ* is an unclassified publication funded by the Weapons Programs Directorate.

Managing Editor-Science Writer
Margaret Burgess

Science Writer-Editor
Jan Torline

Designer-Illustrator
Randy Summers

Editorial Advisor
Jonathan Ventura

Technical Advisor
Sieg Shalles

Printing Coordinator
Lupe Archuleta

Send inquiries, comments, and address changes to nwpub@lanl.gov or to
The Nuclear Weapons Journal
Los Alamos National Laboratory
Mail Stop A121
Los Alamos, NM 87545



**The World's Greatest Science
Protecting America**

Los Alamos National Laboratory, an affirmative action/equal opportunity employer, is operated by Los Alamos National Security, LLC, for the National Nuclear Security Administration of the US Department of Energy under contract DE-AC52-06NA25396.

This publication was prepared as an account of work sponsored by an agency of the US Government. Neither Los Alamos National Security, LLC, the US Government nor any agency thereof, nor any of their employees make any warranty, express or implied, or assume any legal liability or responsibility for the accuracy, completeness, or usefulness of any information, apparatus, product, or process disclosed, or represent that its use would not infringe privately owned rights. Reference herein to any specific commercial product, process, or service by trade name, trademark, manufacturer, or otherwise does not necessarily constitute or imply its endorsement, recommendation, or favoring by Los Alamos National Security, LLC, the US Government, or any agency thereof. The views and opinions of authors expressed herein do not necessarily state or reflect those of Los Alamos National Security, LLC, the US Government, or any agency thereof. Los Alamos National Laboratory strongly supports academic freedom and a researcher's right to publish; as an institution, however, the Laboratory does not endorse the viewpoint of a publication or guarantee its technical correctness.



Fracture and Damage Evolution in Polymers

LANL's Dynamic Behavior of Polymers Team is developing an interdisciplinary research program to quantify the fracture toughness and mechanisms of damage evolution for a variety of polymers. Here we present our baseline test results on four polymers that illustrate the significance of the glass transition temperature and of thermally induced phase transitions on failure mechanisms.

Polymers are found in numerous applications within DOE/NNSA defense programs. Polymers are chosen for a variety of reasons, for example, their desirable and highly tunable mechanical properties, their accommodating and economic manufacturing methods, and their application as the binder phase in composites such as plastic-bonded explosives. However, polymers naturally exhibit low strength and are vulnerable to aging in the form of oxidation, cross-linking, crystallization, morphology evolution, and loss of molecular weight, all of which can change a polymer's mechanical response and resistance to failure or fracture. In order to design against and predict failure, it is essential that scientists understand the fracture response of these materials.

The recognition that all structures are manufactured with, or will ultimately contain, flaws that govern eventual structural failure has led to advanced understanding of material failure. Fracture mechanics studies, originally limited to linear-elastic materials and ductile metals, are increasingly capable of addressing the complexity of nonlinear ductile polymers.

Fracture Toughness

Our fracture mechanics studies employed accurate fracture toughness measurements. Higher fracture toughness equals higher resistance to crack growth, which can be equated to higher performance.

We measured the fracture toughness of the polymers PTFE 7C, Kel-F 81, Kel-F 800, and PEEK 450G as a function of temperature. PTFE is Teflon (polytetrafluoroethylene), commonly known for its "slipperiness," or extremely low coefficient of friction. Kel-F 81 is the trade name for polychlorotrifluoroethylene (PCTFE), which is used in various cryogenic components, valve seats, seals, and microelectronics packaging. Kel-F 800 is a copolymer of 75% PCTFE with 25% polyvinylidene fluoride (PVDF) and is used at LANL as the binder in the plastic-bonded explosive PBX 9502. PEEK 450G is polyetheretherketone, a semicrystalline polymer found in numerous applications that take advantage of its high-temperature performance (e.g., piston parts, bearings, and load-bearing aerospace components).

The high strain to failure (i.e., material failure requires high strain) and the nonlinear response of the four polymers we studied require using a fracture toughness measurement that accurately captures both the elastic and plastic portions of deformation. Fracture toughness is a measurement of the energy required to deform a material, and that deformation ultimately leads to crack propagation. Elastic deformation is reversible; when load is removed, an elastically deformed material returns to its original shape.

In our polymer toughness tests, elastic deformation provides a mechanism for the material to store energy, which drives crack growth with the continuing application of load. In contrast, plastic deformation is a permanent shape change that provides a mechanism for the material to dissipate energy and blunt the crack. Crack tip blunting is a reduction in the sharpness of the crack tip, reducing stress at the crack tip and further increasing energy required for crack growth.

We developed a measurement capability based on the J -integral fracture toughness criterion using elastic-plastic fracture mechanics. J -integral fracture toughness is a material parameter corresponding to the energy required to produce a unit area of new crack surface. In ductile materials, crack extension features three regimes:

- plastic deformation near the crack tip caused by crack tip blunting,
- crack initiation when the strain energy in the sample reaches the critical fracture toughness at which the polymer will give way, and
- crack propagation through the component.

The fracture toughness of PTFE 7C, Kel-F 81, Kel-F 800, and PEEK 450G is approximately 2 orders of magnitude greater than that of glassy, brittle polymers such as Epoxy 828/DETA. The fracture toughness of this epoxy is equal to or greater than that of most glasses, ceramics, and geological materials. In comparison, the fracture toughness of the four polymers we tested is roughly 1 order of magnitude less than that of high-toughness steel such as ferrous alloy 9-4-20 and equivalent to modest-toughness metals such as 7075-T6 aluminum or 4340 steel.

Crack Initiation

Graphing strain energy as a function of crack extension requires knowledge of the crack tip position as a function of applied load. Historically, two primary methods have been employed to determine crack tip position: the multiple specimen method and the compliance method. The multiple specimen method is costly and not practical when material is limited because many samples are required for a single data point. The compliance method, which involves loading and unloading the specimen to infer the crack tip position based on changes in specimen compliance (inverse of stiffness measured at the deformation of a body under a given load), yields an infinite number of solutions without a means to discern the one correct solution in the case of viscoelastic polymers.

Therefore, we employed the normalization method, which uses an analytical solution with power law

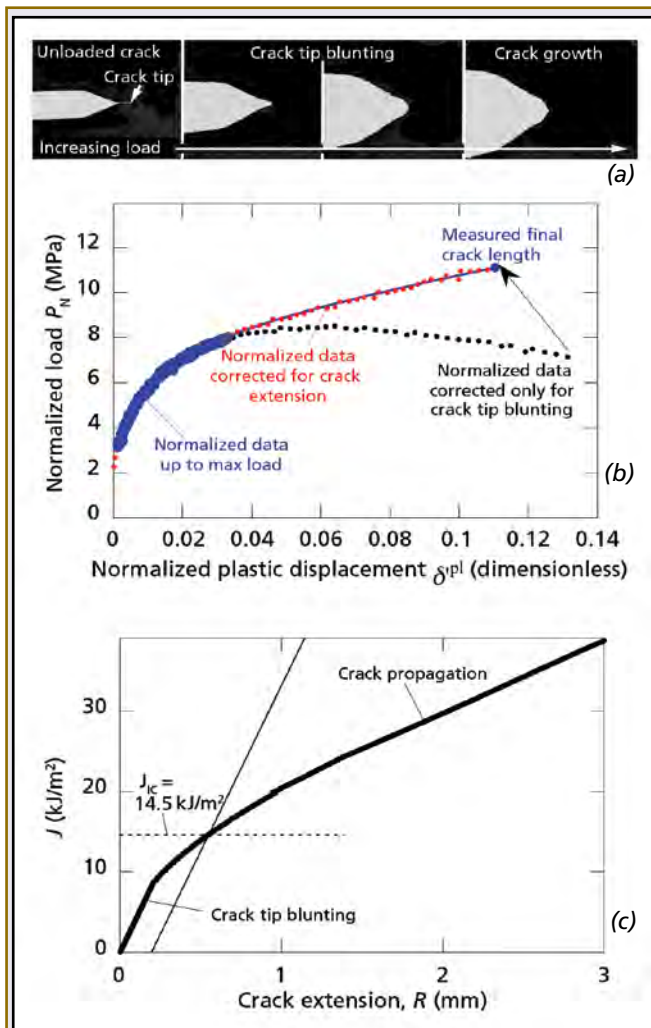
DEFINITIONS

glass transition temperature—The temperature below which molecules have little relative mobility. Many polymers consist of both amorphous and crystalline domains. At their glass transition temperatures, amorphous polymers or the amorphous domains in semicrystalline polymers undergo a phase transition and become hard and brittle, cracking and fracturing like glass rather than undergoing ductile deformation.

phase transition—The change in one or more physical properties of a material resulting from a change in a thermodynamic variable such as temperature or pressure. Molecules collect in three possible physical states—solid, liquid, or gas; phase transitions occur between these physical states. Polymers can undergo temperature- and pressure-dependent phase transitions that signal changes in properties different from those associated with the usual transitions.

Numerical designations signify the order in which polymer phases were discovered. For example, the four distinct crystalline phases of PTFE 7C are designated I, II, III, and IV. The PTFE phase III crystalline structure occurs only at elevated pressures; PTFE phases II, IV, and I denote three different helical windings of the polymer chains.

The order of a phase transition determines whether energy is required for the transition to occur. A first-order transition (e.g., changing how tightly a PTFE 7C polymer chain is wound) involves absorption or release of energy (i.e., latent heat) and change of temperature or pressure. In a second-order transition (e.g., a glass transition, for example), physical properties change at the phase transition, but energy is not absorbed or released.

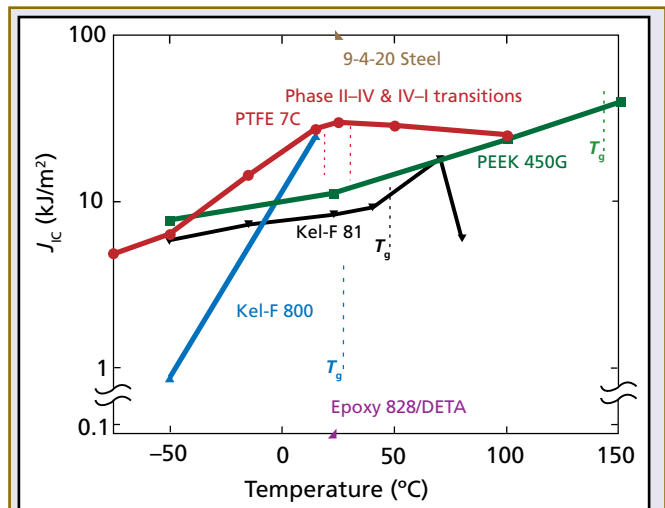


(a) Sequence of crack tip blunting and crack growth. (b) Normalized load–displacement data corrected only for crack tip blunting (black) and then accounting for crack extension (red). (c) The resulting plot of J -integral energy as a function of crack extension (R) is used to determine critical fracture toughness. The initial slope of the resulting curve captures blunting behavior. Deviation from the linear response indicates crack growth. Critical fracture toughness corresponds to the intercept of the crack extension curve with a line of slope equal to the blunting response offset by 0.2 mm.

(an asymptotic scaling relationship of the generic form $y = ax^k$) behavior for tip blunting and crack initiation. It also transitions smoothly to a linear relationship for steady-state crack growth to accurately estimate the position of the crack tip throughout the test.

Temperature Dependence

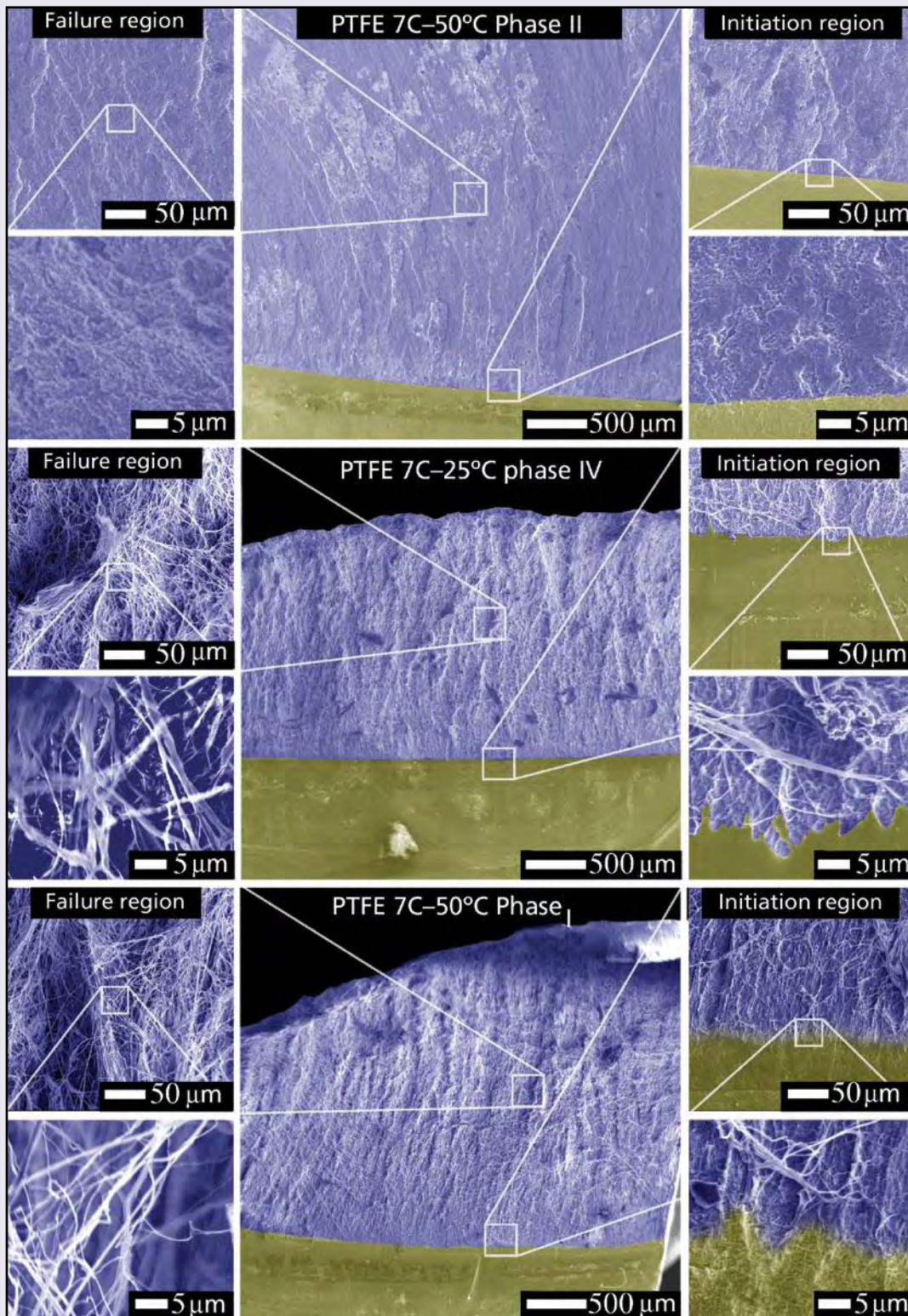
The fracture behavior of the four polymers we studied is strongly dependent on temperature, in some cases changing by more than 1 order of magnitude



Fracture toughness as a function of temperature. Solid lines illustrate fracture toughness as a function of temperature; vertical dashed lines indicate the glass transition temperatures (T_g) and phase transitions. The room-temperature critical fracture toughness (J_{IC}) values of a high-toughness metal (9-4-20 steel) and a glassy, brittle polymer (Epoxy 828/DETA) are also shown.

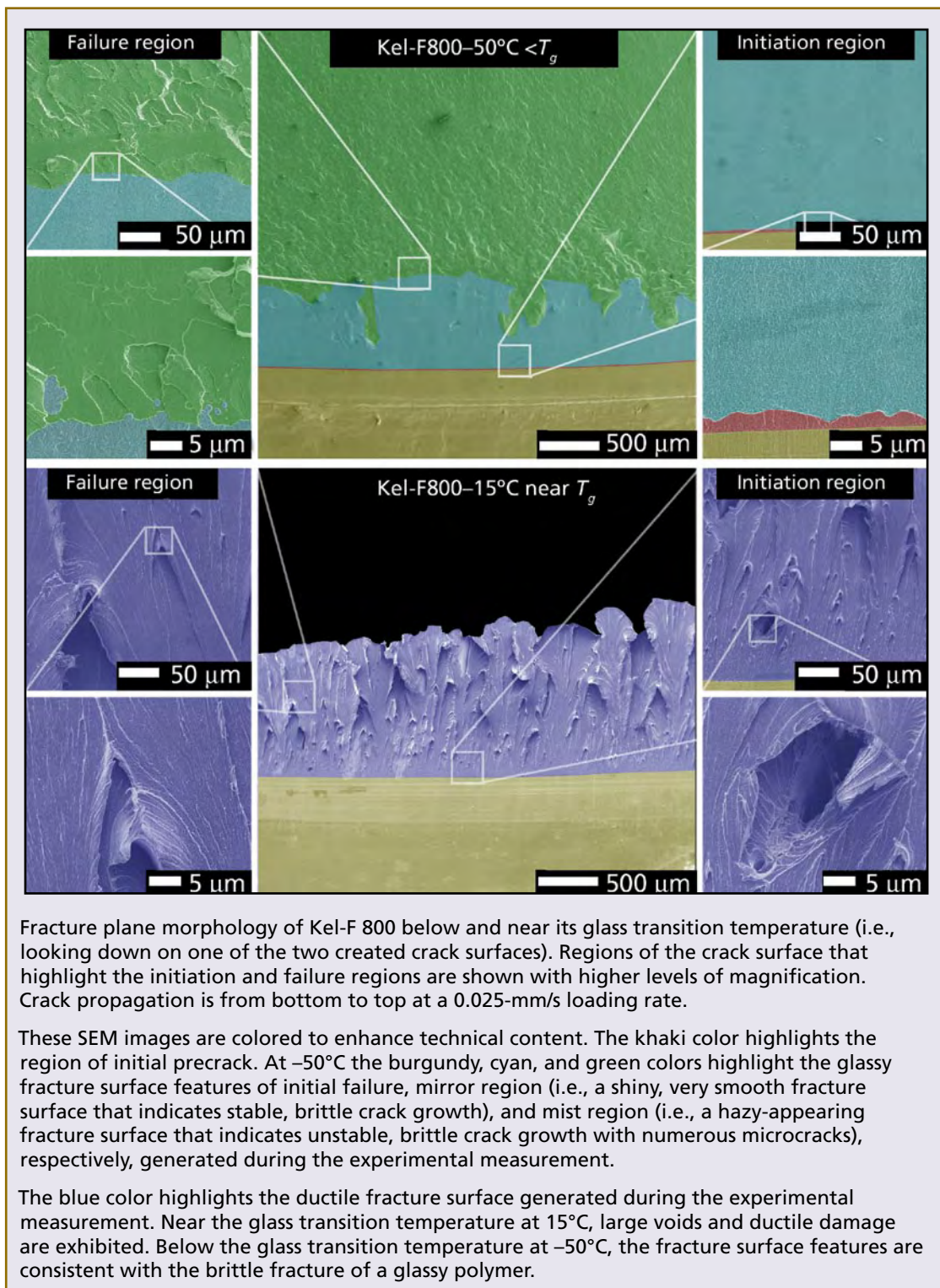
over a normal seasonal temperature range. Their toughness increases with increasing temperature, particularly below their glass transition temperatures. Their fracture behavior can change dramatically above their glass transition temperatures or because of phase transitions.

PTFE 7C exhibits a strong increase in critical fracture toughness with temperature when the crystalline structure is phase II, peaks as it transitions to phase IV, and then decreases with temperature in phase I. Below its glass transition temperature, the temperature dependence of Kel-F 81 is relatively low. Above that temperature, the increased ductility results in a significant increase in the critical fracture toughness at approximately 75°C , followed by a precipitous drop in toughness due to decreasing flow stress. Kel-F 800 exhibits significant toughness as it approaches its glass transition temperature; however, at nominally reduced temperatures, it rapidly becomes a glassy, brittle polymer with low fracture toughness and catastrophic dynamic crack growth. The critical fracture toughness of PEEK 450G has a strong dependence on temperature and there are no significant changes as it passes through its glass transition temperature.



Fracture plane morphology of PTFE 7C in phases II, IV, and I. Crack propagation is from bottom to top at a 0.025-mm/s loading rate (i.e., looking down on one of the two created crack surfaces). Regions of the crack surface highlighting the initiation and failure regions are shown with higher levels of magnification.

These scanning electron microscopy (SEM) images are colored to enhance technical content. The khaki color highlights the region of initial precrack; the blue color highlights the fracture surfaces generated during the experimental measurement. The phase II image displays brittle fracture with cleavage fracture surfaces and nominal local deformation. Phases IV and I demonstrate ductile failure with significant localized deformation in the form of fibrils.

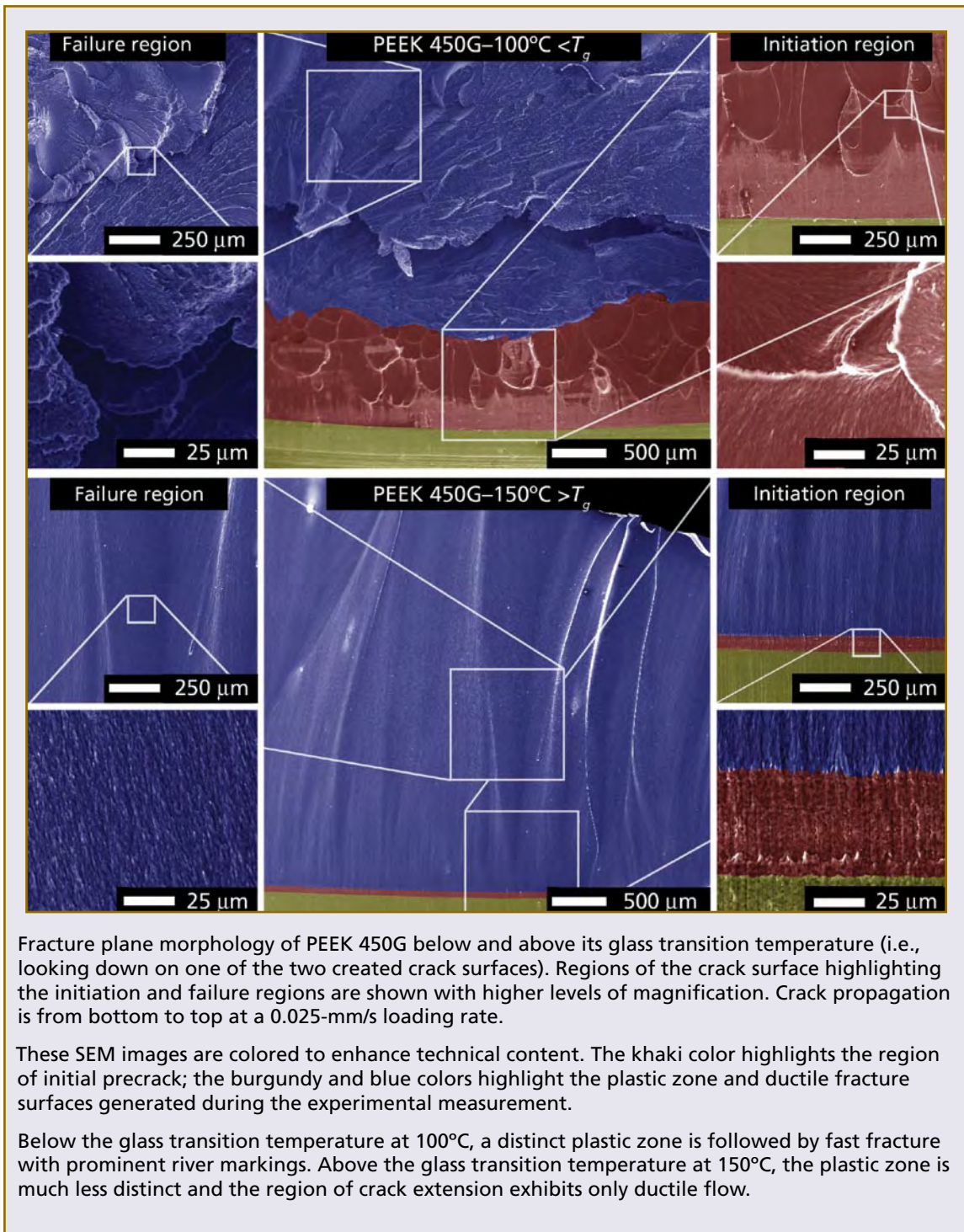


Fracture Morphology

Postmortem investigation of a material fracture surface can provide significant insight into fracture mechanisms and morphological changes that lead to changes in fracture behavior. We obtained scanning electron microscopy (SEM) micrographs of the fracture surface for PTFE 7C in its three ambient pres-

sure phases and for Kel-F 800 and PEEK 450G above and below their glass transition temperatures. We observed changes at the crack tip location from which the crack propagated and in a region where the crack propagated under a semiconstant state.

We observed two major mechanisms in PTFE 7C:



- brittle fracture with cleavage fracture surfaces and nominal local deformation that is representative of microvoid coalescence (damage in the form of a bubble-like void that initiates and grows in size until it links with other voids to fail the material), and
- ductile failure with significant localized deformation in the form of fibrils (minute, thread-like elements).

The brittle fracture morphology of PTFE exhibits greater similarities to metals with crystalline grain structures than to the mirrored morphology (a very smooth fracture surface) of glassy polymers.

The increase in critical fracture toughness of PTFE during the transition from phase II to phase IV correlates closely with the onset of fibril evolution on the fracture surface. During the transition from

phase IV to phase I, we observed that fibrils clearly occur from the immediate point of precrack tip in phase IV, but phase I fibrils are much less defined near the precrack tip.

The dramatic change in fracture toughness in Kel-F 800 is associated with equally dramatic changes in fracture plane morphology. Below its glass transition temperature, Kel-F 800 exhibits a nominal plastic zone with limited plastic deformation. Plastic deformation prior to crack initiation sometimes generates a structural region (the plastic zone) that is unique from the remainder of the fracture surface, which is consistent with the brittle fracture of a glassy polymer.

We observed faint, striation-like marks from interaction of the crack tip with acoustic waves created by crack initiation, which is consistent with the dynamic crack growth. Near its glass transition temperature, Kel-F 800 transitions to highly ductile damage in which microvoid nucleation (bubble formation) and growth dissipates large amounts of energy and bulk plastic deformation blunts the crack.

Below its glass transition temperature, PEEK 450G exhibits a distinct plastic zone that is followed by fast fracture away from the initial crack tip and prominent river markings. River markings are fracture marks that look like a river's tributaries on a map and point to the origin of the crack. The plastic zone consists of ductile flow at the point of crack initiation with numerous radial slow-growth domains (circular features on the fracture surface that indicate formation of a void from which a stable crack grows radially) and coalescence failure processes.

Above its glass transition temperature, PEEK 450G shows no clear plastic zone or noteworthy fracture morphology in the region of constant crack growth rate. Although PEEK 450G retains its toughness above its glass transition temperature, its crack extension mechanisms transition to simple ductile flow instead of cracking.

Approach Results

Our fracture mechanics and damage quantification research, analytical techniques, and model development represent a novel experimental approach that could significantly impact LANL's polymer applications (e.g., explosive charges and structural components). Our results also have potentially significant impacts on industry (e.g., automotive body parts and construction materials), defense (e.g., light armor), and surgical medicine (e.g., joint replacements and dental implants). Our research on fracture origin and development presents an opportunity to reduce the human and financial costs associated with damage evolution that leads to catastrophic failure of polymeric materials. [NWJ](#)

Points of contact:

Eric N. Brown, 667-0799, en_brown@lanl.gov

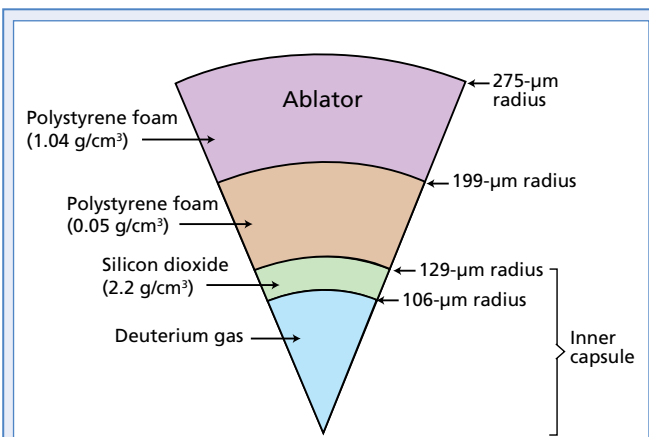
Dana M. Dattelbaum, 667-7329, danadat@lanl.gov

Using Double-Shell Target Experiments to Validate ASC Codes

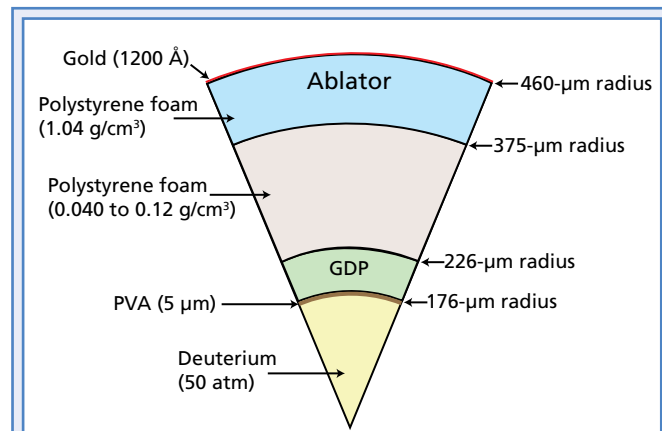
Experiments that validate Advanced Simulation and Computing (ASC) codes and require the use of large lasers—particularly experiments related to stockpile stewardship—can be expensive ventures. Therefore, LANL scientists are exploring cost-effective techniques and targets that can provide excellent research properties. Researchers also need to determine when their results are acceptably complete; i.e., does an experiment address the stockpile stewardship issue under study or is further work required?

LANL Studies

To optimize results in our studies of the ignition of hydrogen isotopes that use lasers configured for inertial confinement fusion, the Complex Implosion Team is examining the implosion properties of double-shell targets that use noncryogenic fuel (noncryogenic fuel is less costly and easier to handle than cryogenic fuel). In these experiments, the low-Z (low atomic number) outer shell of this type



Cutaway view of indirect-drive, spherical double-shell capsule. This standard double-shell target configuration consists of a low-Z outer ablator shell separated from a higher-Z inner shell by low-density polystyrene foam. The outer shell is made from two parts that snap together. The inner shell is a standard glass capsule (target) that contains room-temperature deuterium fuel at high pressure. In indirect drive, a laser beam hits the inside wall of a cylindrical or tetrahedral hohlraum, creating x-rays that hit the outside of the target.



Schematic of a direct-drive double-shell target. The outside of the outer shell was coated with 1200 Å of gold. The inner capsule, with a radius of 226 μm, was a silicon germanium-doped polymer (GDP) glass microballoon, encapsulating a thin-walled polyvinyl alcohol (PVA) microballoon that contained the fuel. These experiments measured the neutron yield from the targets and the x-ray emission images of the compressed target cores. In direct drive, the laser beams are focused directly on the target rather than on the inside wall of a hohlraum. The diagram is not to scale.

of target absorbs incident energy from the x-rays in a hohlraum (an open-ended chamber around the target) in an indirect laser-drive configuration or directly from the laser in a direct-drive configuration. The outer shell then ablates and accelerates inward, imploding on an inner and possibly higher-Z (more incident-energy-trapping) shell that contains a noncryogenic fuel such as room-temperature deuterium. Although the collision is nonelastic, little energy is lost when the two shells collide. As a result of its smaller mass, the inner shell accelerates inward more quickly than the outer shell; compresses the cold, noncryogenic, high-pressure fuel; and heats the fuel to ignition.

This double-shell design is based on a two-part single-shell design: a thin, graded-density beryllium shell and a plastic capsule that contains cryogenic deuterium or deuterium-tritium fuel. The single shell ablates and compresses a cryogenic layer

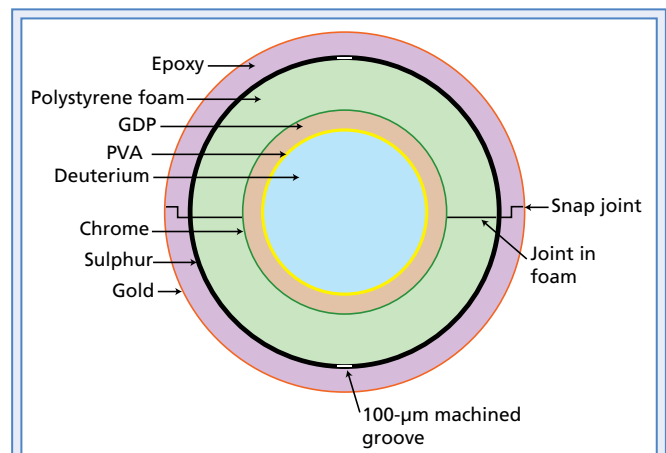
of fuel with four successive shocks to produce a hot spot (localized area of dissipated energy) that is surrounded by a dense fuel assembly.

Although the double-shell configuration is not as hydrodynamically stable as the single-shell design, the double-shell configuration has at least the following advantages over the standard single-shell design.

- It isolates the absorption and ablation process from the implosion process, which lowers the effect of outer-shell instability.
- Its inner shell reduces radiation loss from the fuel and increases confinement (separation) time for the ignited fuel.
- It reduces sensitivity to fuel inhomogeneities or helium-3 bubbles that may occur in cryogenic fuels used in current single-shell targets designed for use at the National Ignition Facility.
- Its ignition timing requirements are less rigorous than those of single-shell designs.
- Its inner-shell implosion velocity is lower than that of the single-shell design.

Although LANL had experimented with double-shell targets in direct and indirect configurations, we had not achieved the yield predicted by our previous 1-D clean calculations, i.e., calculations that did not account for the effects of parts of the shell material mixing with the fuel or for the effects of target asymmetry. Using imaging and reduced absorption targets, we determined the importance of preheat, which reduces the effect of surface machining on image sharpness, caused by M-band radiation in a hohlraum environment. Our measured yield, relative to our calculations of the capsules that did not include mix (the so-called yield over clean ratio [YOC]), was approximately 50%—one of the highest ratios we observed.

These differences in single- and double-shell calculation results prompted further study to understand why only some targets achieved high YOC values. In three studies, therefore, we focused on shell evo-



Direct-drive radiography target. The diagram shows the step (snap) joint in the epoxy ablator and the relative positions of the machined groove, snap joint, and joint between the two polystyrene foam hemishells. The horizontal line that separates the top and bottom parts of the foam layer indicates the joint between the two halves of the foam hemishells. The snap joint and the joint in the foam were aligned in the same plane to reduce their effects on imaging the machined groove as it developed.

lution and collision, how preheat from the gold layer we deposited on the outside of the capsule (the hohlraum) affects the fuel in the capsule, and the effects of potential defects (asymmetries) in a target.

Double-Shell Target Design

A standard double-shell target uses a cylindrical or a tetrahedral hohlraum. Low-density foam separates the two-part, low-Z outer ablator shell from a higher-Z inner shell. The outer shell's two parts snap together. The inner shell is a standard glass capsule that contains room-temperature deuterium fuel at high pressure.

In previous direct-drive, double-shell investigations, we deposited a thin layer of gold on the outside of the capsule (target) to generate variable amounts of M- and L-band radiation and we experimented with a <math><0.5\text{-}\mu\text{m}</math>-cell carbon-resorcinol foam rather than a 1- to 5- $\mu\text{m}</math>-cell polystyrene foam. These experiments measured the neutron yield from the targets and the x-ray emission images of the compressed cores. However, we still needed to determine the critical role of asymmetry on the hydrodynamics of a target and whether the M-band effect correlated with our earlier calculations.$

Our results had shown that

- target construction techniques can affect experiment results,
- then-current targets lacked sufficient energy to obtain high-conversion ratios or high yields,
- smoothing the laser beam irradiance by spectral dispersion (SSD) was not critical to the experiment at then-achievable compressions and yields,
- target-mounting techniques in the hohlraum had little effect on results, and
- varying the cell size of the foam in the target did not produce the effects we expected.

To quantify our understanding of the bulk hydrodynamics of the target and its construction requirements, we designed a direct-drive target that was two times as large as our previous 1-D target. With its layers of sulphur and chromium, our new design allowed us to radiograph the implosion with sufficient resolution that we could measure both shell trajectory and collision. It also validated our calculations because we could better evaluate the effects of

- joint and construction details on implosion symmetry,
- large-sized foam cells on implosion stability, and
- preheat from the thin gold layer we had deposited on the inner shell of our new design.

OMEGA Setup

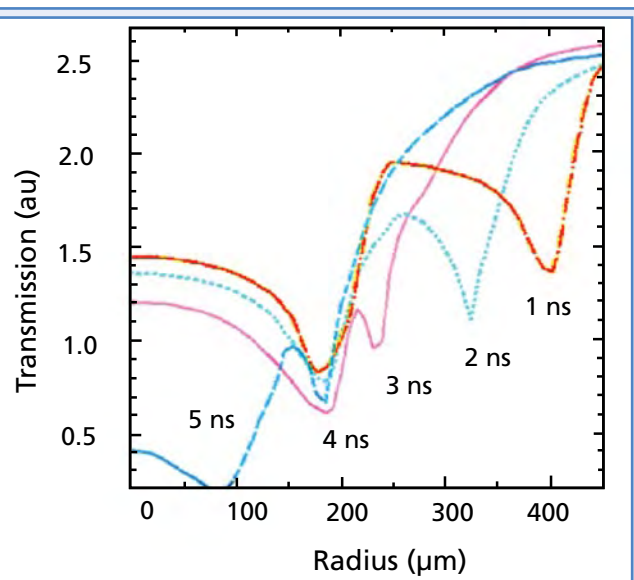
We designed our next double-shell experiment for use on the University of Rochester's Laboratory for Laser Energetics (LLE) OMEGA laser system because OMEGA's 60 laser beams can be directed to a target in 3 separate clusters. Each 20-beam cluster can irradiate a spherical target from all directions to achieve direct-drive, symmetric illumination with the full 60 beams. To utilize the OMEGA configuration, we developed an unconventional design, using 20 beams from 1 cluster to radiograph the target and the other 40 beams (2 clusters) to drive (implode) the target. The design's reduced

energy helped slow implosion, which reduced motional blur in the radiographs.

However, we needed to determine how to (1) irradiate the target with maximum uniformity using this reduced laser energy and (2) use the remaining 40 laser beams efficiently.

To resolve the irradiation issue, we pointed 40 beams (2 clusters) along different positions on the target chamber's vertical axis of symmetry rather than at its center. We selected only four pointing positions, which we placed symmetrically, relative to the center of the chamber and along its vertical axis.

We used the remaining 20 beams (from the third cluster) to radiograph the target with x-rays. Because the beams in each cluster could be used at different times, with different beam conditions, and



Postprocessed simulated transmission lineouts of the radiographs. Colored lines represent x-ray transmission through the imploding target at different times. The positions of the sulphur and germanium-doped polymer layers show clearly as dips in the transmission, which are measured in arbitrary units (au). The sulphur layer causes the dip at the larger radius and the chromium layer causes the dip closer to the origin. The sulphur layer in this experiment enhanced radiographic resolution, enabling measurement and evaluation of shell trajectory and collision, how joints and construction affect implosion symmetry, and the effects of large-cell foam on implosion stability. The chromium layer allowed measurement of preheat from the thin gold layer placed on the inner shell and validated the researchers' previous calculations.

in different directions to illuminate two iron backlighters, we set these beams in the planes of the target seams or joints. A 1-mm, low-magnification field of view provided early-time views of the outer capsule. The second (500- μm) field of view showed the target after collision. The two 6- μm -thick iron backlighters were illuminated by either 6 or 14 laser beams at an irradiance of $2 \times 10^{15} \text{ W/cm}^2$, the optimum for maximum conversion efficiency for iron. We used iron backlighters because iron's x-ray wavelength (color) can distinguish the edges of the target clearly. The backlighter beams were 1-ns, flat-topped pulses with no SSD or distributed polarization rotators. Target images were recorded with fast x-ray framing cameras using gold photocathodes and 200-ps pulsers.

Target Design

The direct-drive radiography target contained seven layers of material, including an outer 86- μm -thick epoxy target shell that we coated with a 1200- \AA layer of gold. The inside 10 to 20 μm of the outer shell was coated with a 4% sulphur dopant that we used as an x-ray marker that we could observe clearly with the iron backlighter. A 50-mg/cm³ polystyrene foam layer separated the sulphur layer from the foam inner shell. A 47- μm -thick capsule of germanium-doped polymer (GDP) shell enclosed a thin polyvinyl alcohol (PVA) spherical capsule. The inner capsule contained fuel (room-temperature deuterium gas) at pressures of 0 to 50 atm.

Target Hydrodynamics

Target defects—small target asymmetries that potentially could limit implosion symmetry—also may reduce implosion yield.

To simulate potential asymmetry that could affect target hydrodynamics, we machined a groove along the doped (inside) epoxy layer and conducted Radiation Adaptive Computer Grid Eulerian (RAGE) computer simulations on the double-shell implosion before and after machining the groove. The machined groove helped us determine whether our calculations were extensive enough to account for inevitable target imperfections but still ensure design success.

However, because RAGE does not account for laser energy sources, we also used a 1-D LASNEX Lagrangian computer code to simulate the x-ray drive and x-ray preheating of the capsule that resulted from M-band x-ray radiation emitted from the 1200- \AA -thick gold layer.

Using the LASNEX simulation to determine the amount of laser energy deposited into the capsule ablator and estimating the depth of that energy (approximately 9 to 10 μm), we determined the laser drive energy source. Then we applied the corresponding mass-specific energy source to an outer layer of the capsule ablator in the RAGE simulation.

To determine x-ray preheat energy sources, we used the LASNEX simulation to extract the change in the mass-specific internal energy of the capsule interior (the gas fill, inner shell, foam region, and outer shell except for the laser deposition layer) as a function of radius and time. To incorporate these data into the RAGE simulation, we divided the capsule interior into many regions, working from the center of the capsule to the laser drive (outermost) layer. LASNEX then determined the mass-specific energy source for each region.

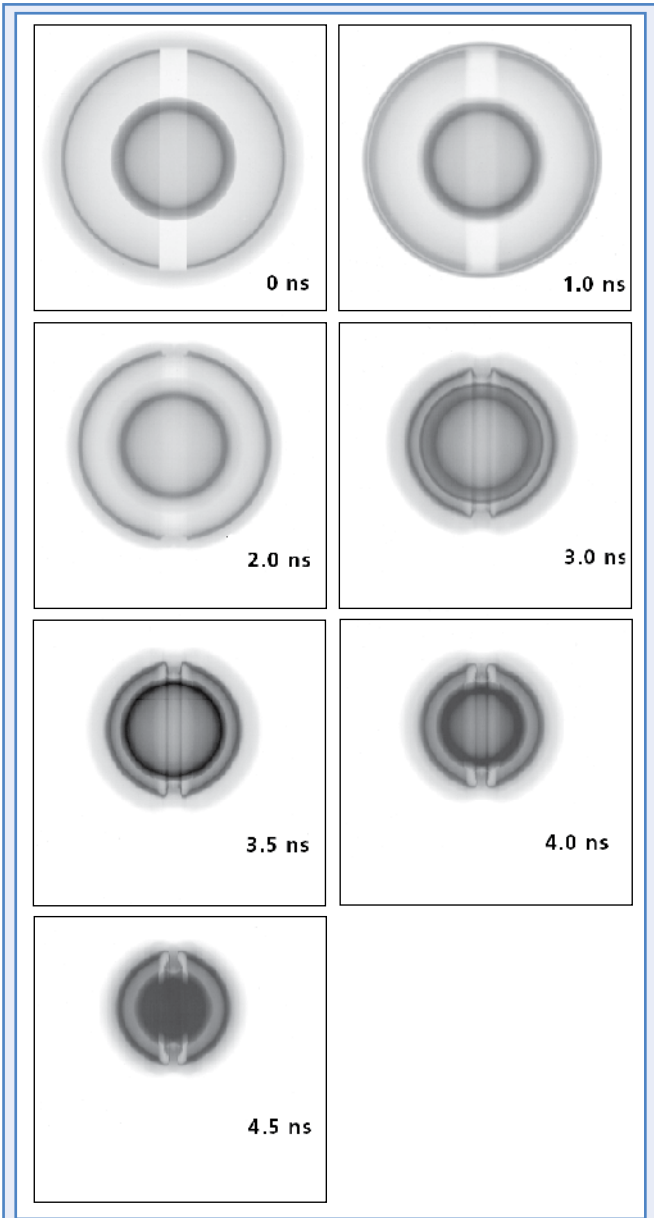
Groove Effect

In previous studies of the motion of the outer shell, in which we used a nongrooved target, our calculations matched our simulation measurements. In other cases, we added grooves to the target, which required us to increase the germanium-doped epoxy thickness to 15 μm . We then added a chromium layer to the inner target to observe the trajectory of the inner shell surface.

Working with a machined, 100- μm -wide groove but no chromium on the inner layer, we observed the initial shock in the ablation layer at 1 ns. At 3 ns, the sulphur layer and the developed perturbation from the groove had not interacted with the inner germanium-doped layer. By 3.5 ns, the groove began to affect the stability of the inner capsule and implosion began. By 4 ns, we observed the effect of the groove on the inner capsule. By 4.5 ns, the imploded capsule was too thick to be observed in

these calculations, although the effect of the groove changed little.

As we observed the effect of the groove both with and without a chromium layer, we saw that the effect was much easier to resolve, i.e., more visible, using the edge-enhancing chromium layer. The snap joint between the two outer hemispheres caused a perturbation in the chromium surface that was almost as large as that from the machined groove.

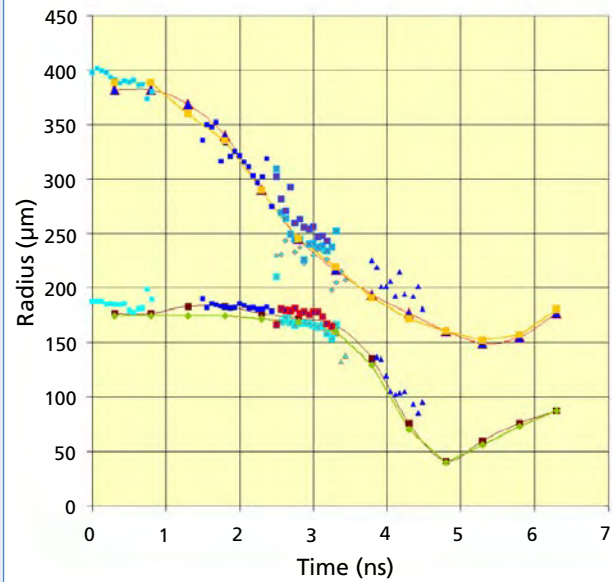


Calculated implosion radiograms, postprocessed from the codes. Shock in the ablation layer was first observed at 1 ns. By 4 ns, the effect of the machined groove could be seen on the inner capsule. By 4.5 ns, the imploded capsule was too thick to be observed in these calculations using the iron backlighter radiation.

The topology of a groove-caused depression in the chromium-layered capsule differed in detail from our postprocessed calculations. Interestingly, the snap joint produces a perturbation like that calculated for the groove. The simulation did not include the snap-joint effect, which will be investigated in future calculations.

Results

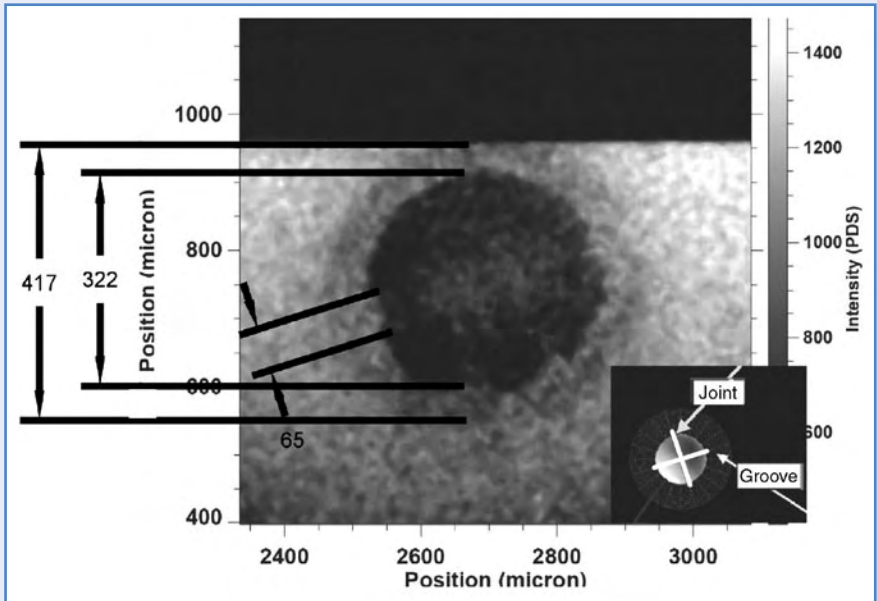
Our OMEGA experiments validated our design for a basic platform that drives an acceptably symmetric implosion of a double-shell target as it diagnoses, with x-ray backlighting, an implosion from two almost orthogonal and independent directions.



Measured and simulated trajectory of peak absorption features for the nonchromium, imploding double-shell targets. The upper trajectory (gold line) tracks the dip in the transmission caused by sulphur absorption, and the lower trajectory (green line) tracks the transmission dip in the GDP layer. Trajectory positions were found by azimuthally averaging the images around a best-center position, which simultaneously minimized fit error to the dip in the trajectory by using an elliptical or a circular fit to the radiograms.

Ellipticity generally was small at early times and was significant only after 3.5 ns; postprocessed calculations are shown with different laser energies. The estimated time uncertainty is approximately 60 ps; estimated error in each measured radius is less than $\pm 5 \mu\text{m}$. The data spread is larger than each individual measurement because the figure shows several camera shots (indicated by colored symbols on or near trajectory lines) at different preheat levels from 600 or 1200 Å of gold as well as other shots with a gas fill of 0 or 50 atm deuterium.

Radiogram of an imploding target at 3.84 ns. The inlay shows the view of the camera relative to some features in the target. Note the machined groove (*bottom left to top right*) and the seam in the target (*bottom right to top left*). The faint ring is the imploding outer shell; the inner black object is the outline of the chromium-covered capsule. The radiogram shows two interesting features. The feature at the bottom left, observed by a detector in the planes of the groove and the snap joint, is due to the premachined groove in the outer shell. The feature at top and right is due to the snap joint between the two outer hemispheres, which caused a perturbation in the chromium surface almost as large as the perturbation from the machined groove. Although the radiogram shows the perturbation in the sulphur layer, the image is not sufficient to resolve the perturbation in the foam. Inset (*bottom right*) shows locations of the snap joint and the machined groove. Intensity is measured in photodensitometer system (PDS) units.

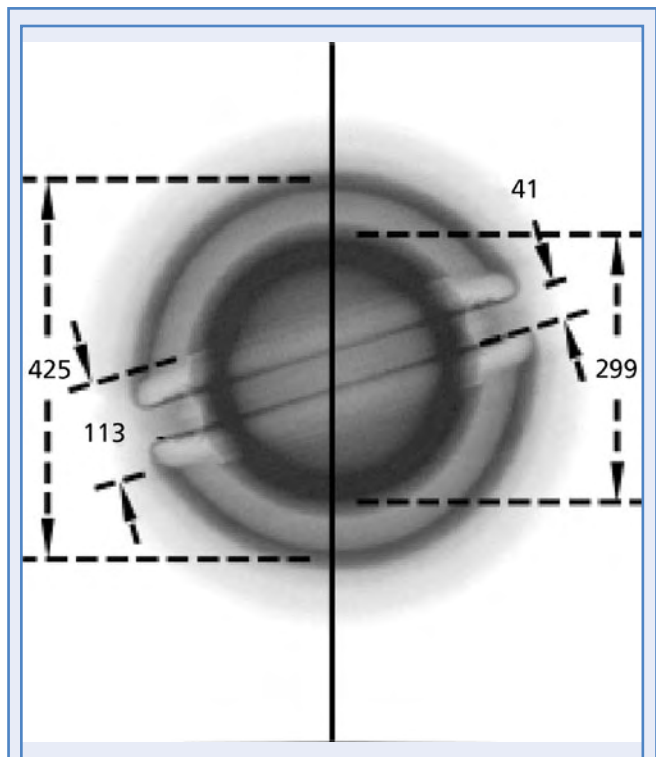


These experiments also were successfully used to validate ASC codes.

Experimenting with these compressible, convergent plasma shells, we demonstrated that our hydrodynamic modeling agrees with our measurements of the bulk hydrodynamics during the time (0 to 4.5 ns) we were able to observe the shells well. Confirming turnaround time (the time at which the inner shell achieves minimum radius before expanding again) will be difficult because the core emission radiance of the burning deuterium fuel greatly exceeds all the current x-ray flux that a backlighter can provide.


By creating an exaggerated defect in the ablator, we proved that features smaller than those that we imposed intentionally can significantly affect the trajectory and symmetry of both the inner and outer shells. Our calculations reproduced the general shapes of the implosion but disagreed with simulation details.

We also proved that we can conduct a double-shell implosion experiment and at the same time diagnose the implosion using currently available lasers—



Predicted radiogram using RAGE. Target does not have a chromium shell. The simulated radiogram was calculated at 4.0 ns, and the image was manipulated slightly to show the features clearly. The outer, 425- μ m dark ring is the sulphur layer in the outer epoxy shell. The inner ring is the imploding capsule (all measurements in micrometers).

including those not constructed or optimized for such applications.

Finally, in this first measurement of the time history of a collision of two shells in a double-shell capsule, we showed that employing increased laser energy for both the drive and the radiography and using more-sophisticated x-ray imagers would improve results for this type of experiment. 

Point of Contact:

George Kyrala, 667-7649, gak@lanl.gov

Other contributors to this work include Mark A. Gunderson, Norman D. Delamater, Donald A. Haynes, Doug C. Wilson, Joyce A. Guzik, Ken Klare, Derek Schmidt, Joyce Elliot, Norman Elliot, Laida Valdez, Doug Hatch, R. Blaine, Robert Dean Day, Art Nobile, Scott Evans, Tom Sedillo, Joseph Cowan, Bernhard Carpenter, and Nick Lanier (LANL); Chuck Sorce and Gail Glendinning (LLNL); and the OMEGA operations crew and Steve Craxton (LLE).

NNSA Award

In October 2006, the Complex Implosion Team received a 2005 NNSA Defense Programs Award of Excellence for its significant contributions to the Stockpile Stewardship Program through its creation of an experimental and theoretical platform to validate hydrodynamic modeling in ASC codes using a laser facility.

Led by George Kyrala, the effort involved “. . . precision machining of a complicated, complex target and accurate metrology of a multi-shell target . . .” and developing “. . . accurate image analysis techniques . . .” and a “. . . novel radiography design that provides high spatial and temporal resolution of the shells . . .” The work was noted as “. . . an excellent example of the application of the scientific method to validation . . .” and has been recognized internationally.

DEFINITIONS

clean calculation—Calculation that does not account for the effects of mix.

cryogenic—Of or relating to cold temperatures.

hohlraum—Open-ended chamber around the target that collects the laser light and converts the light to x-rays.

incident laser energy—Amount of energy in a laser beam.

indirect drive—The laser hits the wall of the hohlraum, creating x-rays that hit the target.

inertial confinement fusion—Fuel is adiabatically confined and compressed by moving material.

L- and M-band radiation—Types of x-ray radiation emitted from the different electronic shells in an atom.

laser direct drive—The laser hits a target directly.

mix—Occurs when part of the shell material mixes with the target fuel.

nonelastic—Some kinetic energy in a collision is converted to heat.

preheat—The small amount of heat applied to a target before shock or hydrodynamic motion occurs.

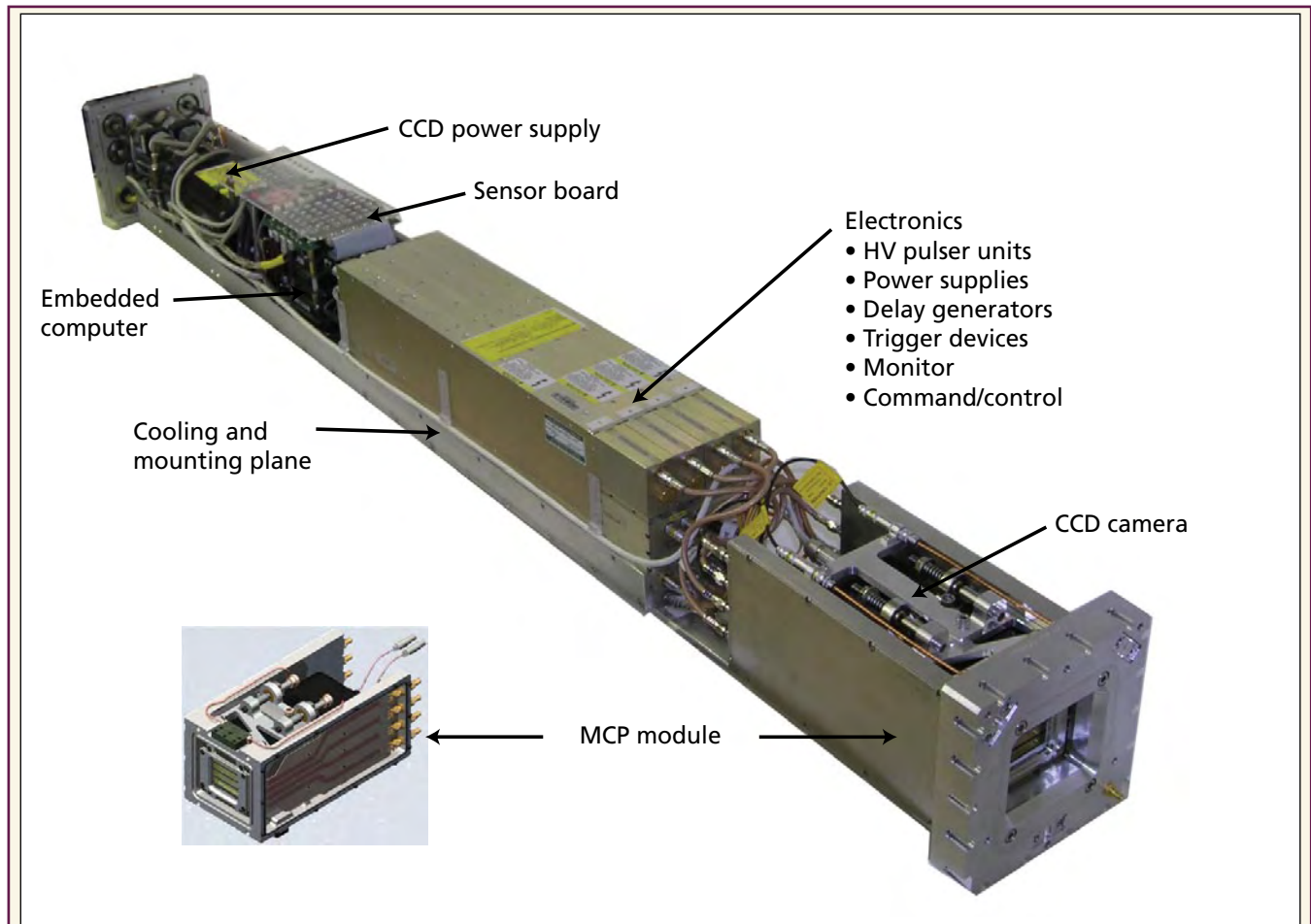
RAGE—Radiation Adaptive Computer Grid Eulerian; a multidimensional Eulerian radiation hydrodynamics computer code with a continuously adaptive mesh refinement capability.

Z number—Nuclear charge number based on the number of protons in the nucleus.

Gated X-Ray Detector for the NIF

The gated (time-dependent) x-ray detector (GXD) LANL designed for LLNL's National Ignition Facility (NIF) is significantly different from earlier generations of gated x-ray imagers due to an innovative impedance matching scheme, improved electrical impedance transformation, pulsed phosphor high-voltage circuits, precision fixturing (assembly) of modular components, unique system monitoring, and remote computer control. The entire instrument fits snugly inside a protective aluminum airbox that also contains an array of environmental sensors.

Designed by LANL scientists and engineers to incorporate 21st-century technology, this next-generation x-ray imager has many advantages over previous GXD designs: it provides a larger image plane that enables researchers to fully image objects with high spatial resolution, allows space on the imaging strip (strip line) for slight misalignments, and slightly increases temporal coverage (image acquisition time). A charged-couple device (CCD) camera records images—it requires no film—operates by remote control to allow last-minute configurations



Gated x-ray detector system. All GXD components are housed in an aluminum airbox, which is electrically grounded in the NIF but electrically isolated from the NIF chamber. The box protects the instrument from data corruption or damage from potential electrical magnetic impulses. The modular design enables disassembly, reconditioning, and reassembly for reuse.

before a shot. The system is designed to be disassembled for reconditioning (most components are off-the-shelf and interchangeable), reassembled, and used repeatedly, and requires less recovery time between shots.

Preliminary characterization tests have shown repeatable uniformity between imaging strips and improved spatial resolution with no detectable impedance reflections.

Gated x-ray imaging cameras commonly used by the international inertial confinement fusion and high-

energy-density physics communities are time-dependent, 2-D imagers. These cameras are important to researchers who require many sequential image frames, with adjustable temporal resolutions from 40 ps to several nanoseconds, spatial resolution of 5 μm , high spectral sensitivity (the detector response to radiation as a function of wavelength), a sensitivity response (dynamic range) of several orders of magnitude, and centimeter-scale image size. Primarily used at large laser facilities, these GXDs are either mounted on a vacuum flange or loaded into an insertable mechanism and translated (positioned) inside a vacuum target chamber.

LANL Design Improvements

LANL's advanced GXD has five basic electrical and mechanical components:

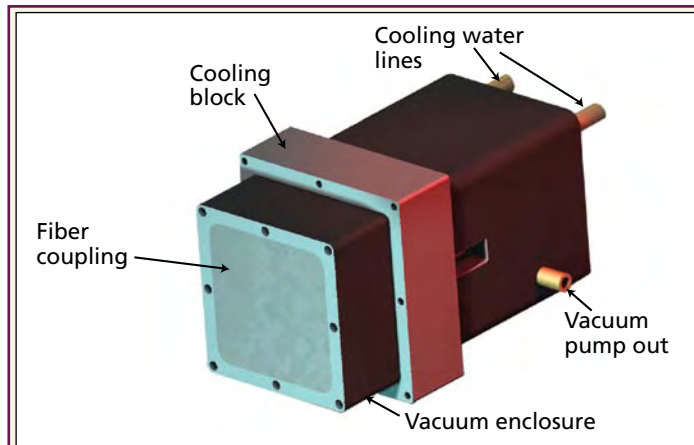
- an aluminum airbox that protects the instrument's sensitive electronics,

- a cooling plane mounting structure that cools all the other parts by thermal conduction),
- a microchannel plate (MCP) module and CCD camera system,
- a gating electronics package, and
- an onboard computer and a sensor package that monitors the GXD internal environment.

The GXD interfaces with the NIF's target chamber through a diagnostic instrument manipulator

(DIM); it also could be used at the University of Rochester's OMEGA laser facility's 10-in. manipulator (TIM). Both the NIF and the OMEGA facility allow the GXD to be put under vacuum and positioned inside the target chamber where it is aligned and readied for data acquisition tasks. A cable bundle containing cooling-water lines, 28-Vdc power, fiber-optic triggers, monitor, and Ethernet leads from the instrument airbox through vacuum feed-throughs in the DIM and out to the facility infrastructure. Instrument operations are compatible with the NIF 2-hr shot cycle, permit remote instrument monitoring, and can fine-tune system MCP sensitivity, timing, and monitor health (temperature, pressure, vacuum, voltage, and current).

After a user places a spectrometer or imaging optic (nose cone) and configures the GXD, the spectrometer or imaging optic is positioned in the target chamber. The GXD and the NIF communicate



CCD camera. To capture an image electronically, a liquid-cooled CCD camera is fiber-optically coupled to the back of the MCP module, which is held in place by three lightweight springs that allow it to float and autolocate on the back of the faceplate. Following confirmation of GXD functionality, a sensor monitor coordinates the NIF timing system with the shot countdown or NIF shot life cycle requirements and acquires and stores a background image. At shot time, optical triggers go to the GXD pulser, phosphor scanner, and CCD camera, and an analog monitoring signal goes to a digitizing oscilloscope in the NIF. The CCD camera reads and stores all data.

through an Ethernet-based diagnostic computer that is located in the target bay. This computer also is the liaison between the front-end processor and the GXD camera. Following confirmation of GXD functionality and system health, the GXD sensor monitor checks the NIF integrated timing system (ITS) for the shot countdown or life cycle; the CCD camera acquires a background image and stores the data by remote control in a secure location. At shot time, optical triggers are transmitted to the GXD pulser, phosphor, and CCD camera, and analog trigger monitor data go to a digitizing oscilloscope located in a shielded area in the NIF. All camera settings are in a hierarchical data format (HDF) of approximately 40 MB per shot. At the same time, the GXD sensor monitor continues to check system health and periodically polls, logs, and displays these data in the diagnostic control room station. If a critical parameter is out of range, an initial warning displays; if the error continues, the GXD is programmed to shut down.

Airbox

The GXD houses all its components in a 6.5-in.-tall x 6.5-in.-wide x 58-in.-long aluminum airbox that weighs 138 lb when it is fully loaded. The airbox is electrically grounded in the NIF through a cable bundle, but electrically isolated from the NIF chamber.

Although the DIM can accommodate instruments much larger than this, researchers wanted the option of operating up to four instruments in the same DIM.

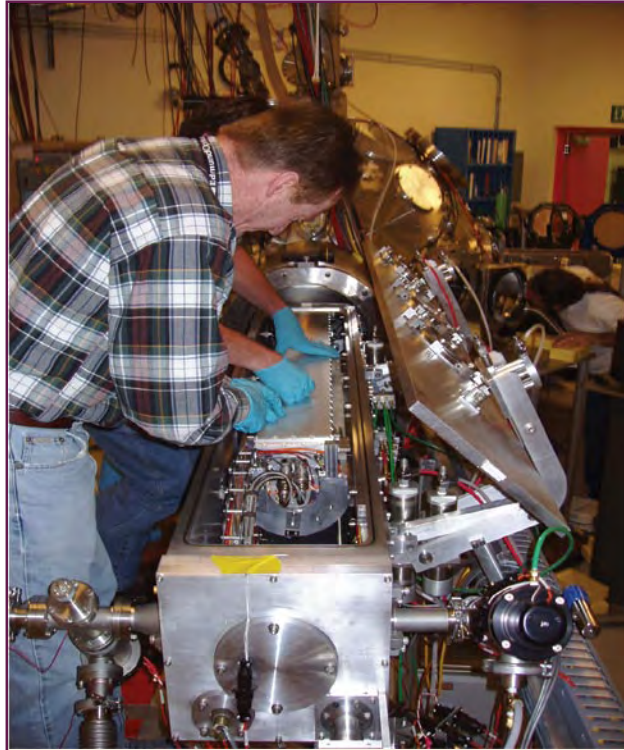
The airbox design protects the instrument from data corruption or damage that could result from

potential electromagnetic impulses; 1 atm of air inside the airbox cools the electronic components better than was possible in earlier vacuum designs. The airbox also protects the components from the NIF operating environment (a neutron flux of 10^{13} at 1.5 m from the center of the target chamber, unconverted laser light up to 100 kJ of $1.06 \mu\text{m}$, a vacuum of less than 4×10^{-5} torr, and a magnetic field of 1 G), which is more harsh (also due to its approximately 2 MJ of laser energy) than the operating environments of earlier generations of these instruments.

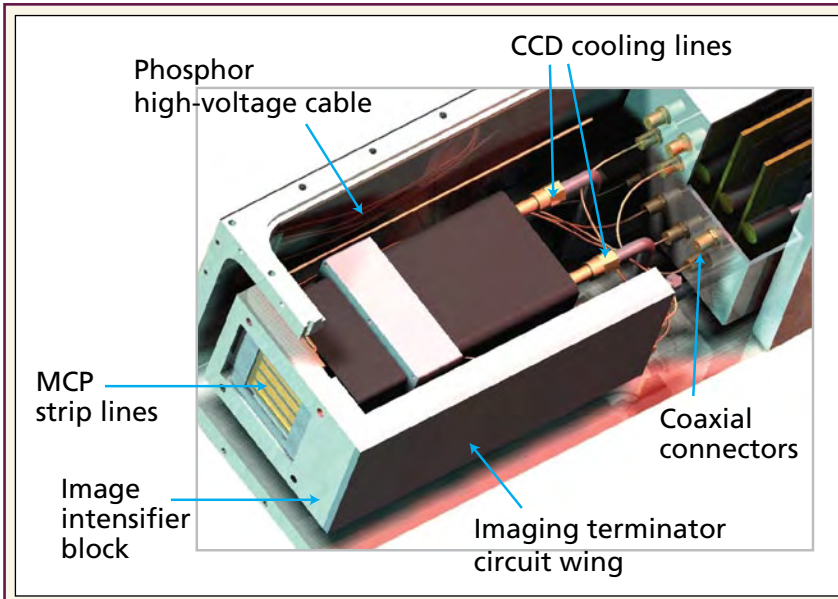
Cooling Plane

Because NIF engineers were concerned that differential heating of the target positioner (a device that holds and positions the target before the shot) could cause target alignment errors, the LANL design restricts heat dissipation into the target chamber to no more than 10 W through the use of the thermal cooling plane, which heat-sinks all heat-generating components.

During preliminary characterization tests, with the cooling plane receiving 1.03 L/min of water at 12.7°C , all components came to thermal equilibrium within minutes of power-up. When the cooling water was completely turned off, the system heated as expected, but did not reach the critical shutdown temperature of 65°C for more than 120 min. This delay to shutdown time is important in GXD operations: if the cooling-water system malfunctions, the GXD can still acquire data for as long as 2 hr before the system shuts itself down.



Characterization experiments. A LANL technician assembles the GXD in preparation for preliminary tests at the Los Alamos Trident facility. LANL engineered the GXD to fit in an aluminum airbox that protects the instrument's sensitive electronics. The airbox also meets the NIF's strict cleanliness and material-compatibility specifications and guidelines.



Microchannel plate module. All components are off-the-shelf and interchangeable. The critical components that establish the space between the MCP and FOFP are machined to at least 0.001-in. tolerance and electropolished and cleaned in an ultrasonic alcohol bath before they are transferred to the clean room where the module components are assembled.

Custom-designed fixtures allow meticulous control of each component; a laser-based proximity sensor measures each placement process. After assembly, the MCP module is stored in a positive-pressure nitrogen dry box to prevent contamination from moisture.

MCP Module

The GXD acquires a time-dependent image by propagating a high-voltage gated pulse across a microwave electrical transmission line that is deposited on the front surface of an MCP. Electrons liberated from the gold photocathode are amplified in the MCP and are electrooptically focused onto a P-43 phosphor-coated fiber-optic faceplate (FOFP).

The LANL system is unique because it has an improved impedance matching scheme that maximizes the transfer of energy but minimizes distortion, a high spatial resolution phosphor screen, and precision assembly fixturing that ensures consistently accurate component alignment, and it can gate the phosphor voltage (earlier designs have direct-current phosphor voltages). Past impedance matching systems used either a direct ohmic mismatch or a shaped transmission line. LANL's GXD uses a printed circuit, surface-mounted impedance transformer that tapers strip impedance from 50 Ω to 10 Ω . This impedance transition minimizes reflections back to the gate pulse source and optimizes energy going to the strip line. The cathodic (electrochemical) deposition technique used on the FOFP results in a very uniform, small-particle-size coating that is very durable and produces greatly improved spatial resolution. Three small, unique, fiducial reference marks on the back of the FOFP allow researchers to easily determine image orientation in their electronic files.

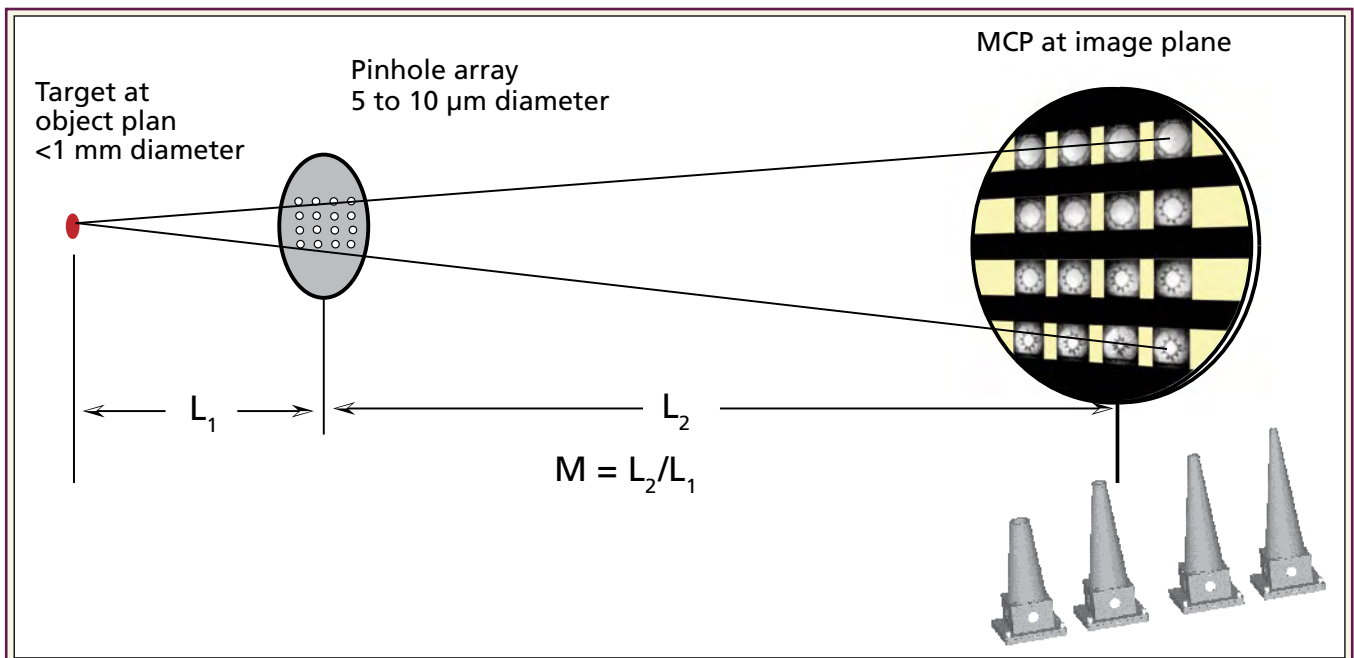
Although not completely unique to these types of diagnostics, pulsing the phosphor screen for improved spatial resolution is rare. Pulsing the phosphor screen voltage rather than direct-current biasing has the advantage of increasing the electrical field between the MCP and FOFP. This change minimizes the transverse energy of the electrons but avoids electrical breakdown between the two surfaces. The optimum pulse width of 10 μ s

Improved GXD design enhances
imaging potential, enables parts reuse,
and operates by remote control.

was determined to be the point, well before breakdown between the MCP and faceplate surfaces, that allowed the voltage to be as high as 5 kV at 0.5 mm plate separation (an electrical field of 1×10^7 V/m).

Gating Electronics

Designed to operate in air rather than in a vacuum, the GXD electronics are computer-controlled. The package includes four gating modules that have an output of approximately 3 kV each with an electrical gate width of 0.2 to 1 ns using changeable, electrically passive pulse-forming modules. These electronic waveforms can be delayed up to 44 ns each in 25-ps increments. Also included are four separate direct-current-bias power supplies for independently modifying the sensitivity gain on each



Operational principle. An array of pinholes on high-Z substrate such as tantalum is placed between the target and imaging plane. By launching a short-duration, high-voltage electrical pulse across an imaging strip line, scientists can produce a photoelectron signal at the front surface of an MCP photocathode. The signal is amplified during transit time of the voltage pulse across a given point on an imaging strip. Varying the width of the electrical gate pulse will vary the corresponding optical gate (i.e., the shutter) time. The level of magnification depends on the location of the pinholes relative to the target. In this graphic, M represents magnification. L_1 is the distance from the target to the pinhole array and L_2 is the distance from the pinhole array to the imaging plane, making the ratio of magnification $M = L_2/L_1$. Nose cones (*lower right*) hold the pinhole array at different distances from the target.

strip line, plus direct-current and pulsed-power supplies for the phosphor screen and photoconductive detector (PCD). Finally, a multiplexed monitor circuit combines the output of the pulsers, pulsed phosphor screen, and PCD that feeds to a high-bandwidth oscilloscope.

Control Software

Most GXD electrical functions are computer-controlled to allow rapid adjustment to system sensitivity between shots and to provide remote voltage and current monitoring. The GXD incorporates electronic readouts and controls wherever possible, and an automated system manages remote-control setting changes. Diagnostic elements are compatible with the NIF's 2-hr shot cycle, can store 400 MB of data per shot, and collect classified data.

Performance

Initial performance characterization measurements show good repeatable uniformity between imaging strip lines, improved spatial resolution, and no

detectable impedance reflections. Additionally, the spatial resolution and signal-to-noise improvements have allowed researchers to observe plasma physics details never before observed. [NWJ](#)

Point of contact:

John A. Oertel, 665-3246, oertel@lanl.gov

Other contributors to this work are Robert Aragonese, Tom Archuleta, Cris Barnes, Larry Casper, Valerie Fatherley, Todd Heinrichs, Robert King, Doug Landers, Frank Lopez, Phillip Sanchez, George Sandoval, Lou Schrank, and Peter Walsh (LANL); Perry Bell, Matt Brown, Robert Costa, Joe Holder, and Sam Montelongo (LLNL); Neal Pederson (VI Control Systems Ltd.); the P-24 Diagnostic and Systems Engineering Team; and the LANL Trident laser operations crew.

UNICORN Experiments Yield Crucial Data

The subcritical (subcrit) experiment UNICORN Realtime Network Anomaly Detection and Intrusion Reporter (UNICORN) is furnishing crucial data about the final plutonium response function that is directly related to a Los Alamos-produced pit. Such data provide important information that allows certification of a pit constructed by LANL's pit-manufacturing processes, a key data set for the Nuclear Weapons Complex.

Pits are hollow spheres of plutonium encased in layers of steel and other metals. The metallic shells are located inside the fission component of modern nuclear weapons, including the W88, which sits atop a Trident II missile.

Subcrit tests such as UNICORN, which was conducted at Nevada Test Site (NTS) in September 2006, involve smaller amounts of plutonium than are required for a self-sustaining nuclear chain



Covered shot hole. UNICORN apparatus and diagnostics were lowered into a 600-ft-deep hole and covered with gravel, concrete, and a bulky, protective steel cover. The detonated HE compresses (implodes) the pit mockup, the compressed pit that contains a subcritical mass of plutonium. Subcritical experiments are defined by their restricted use of plutonium: the quantity used in the tests is safely below the critical mass required for a self-sustaining nuclear chain reaction, ensuring the prevention of a nuclear explosion.



Miles of cables. Approximately 200 cables conducted signals from pin dome diagnostic sensors into a data collection bunker. As is customary in such experiments, UNICORN required many different diagnostic sensors. A pin dome that organized an array of pins of thin electrically conducting wires was a primary data-collection tool. Charged with a significant voltage, the pin wires send an electrical signal when they are electrically shorted by moving surfaces within the imploding pit mockup.

Examining the time distribution at which these signaling events occur allows investigators to reconstruct motion events in the pit as it implodes. The team also used fiber-optic lines to deliver laser light to moving surfaces within the implosion and recombined the reflected light with reference beams. The out-of-phase beams produced optical interference effects from which experimenters deduced the instantaneous velocity of the moving surfaces reflected by the light beams.

reaction. Although subcrit tests provide excellent data, they cannot result in nuclear explosion.

After assembly in vertical racks within an existing onsite tower at NTS, UNICORN diagnostic equipment and instruments were lowered into a 600-ft-deep shot hole, where they were covered with gravel and concrete. High explosives (HE) compressed (imploded) the pit mockup that contained a subcritical mass of plutonium.

Approximately 200 cables conducted signals from pin dome diagnostic sensors into a data-collection bunker.

The pin dome organized an array of extremely thin wire pins, which sent an electrical signal as the wires were electrically shorted by the moving surfaces in the pit mockup as it imploded. Examining the time distributions of these signaling events allowed investigators to reconstruct motion events in the imploding pit. In addition, the scientists employed a so-called photon Doppler velocimetry technique that uses fiber-optic lines to deliver laser light to the moving surfaces and recombines the reflected light from these surfaces with reference beams. Out of phase because they have traveled slightly different distances from source to detector, these light beams produce optical interference effects from which experimenters can calculate the velocities of the moving surfaces that reflected the light beams.

Subcrit tests safely provide crucial pit certification data.

A series of foil switches characterized the details of the burning HE. In subcrit experiments, the HE burn first leads to closure of the foil switches and then signals an instrument that detects the exact timing of the switch closures. By strategically placing a set of such switches around the HE surrounding the experiment, researchers can measure the many diagnostic parameters of the HE burn.

UNICORN was an enormous operational undertaking. Over a 6-year period, the project engaged approximately 500 workers from more than 5 LANL divisions, NTS, 4 national laboratories (LANL, Sandia National Laboratories, Lawrence Livermore National Laboratory, and Pacific Northwest National Laboratory), and Wackenhut Securities. [NWJ](#)

Points of contact:

Gene Christensen, 702-295-4400, genec@lanl.gov

Rendell Carver, 667-0121, rc@lanl.gov



Rack inside tower. After delivery by a secure device-transport vehicle, the experiment and its diagnostics were assembled in vertical arrays (racks) within an existing onsite tower at NTS. Subcritical experiments examine the behavior of plutonium shocked by forces produced by HE chemicals. These experiments produce essential data and technical information that LANL scientists use to maintain the safety and reliability of the nuclear weapons stockpile—a crucial Laboratory stockpile stewardship mission.



Testing the rack-mounted stemming sensor. Before it was lowered into the shot hole, all diagnostic equipment in the rack was tested for its reliability, accuracy, and safety. LANL scientists are using UNICORN data to validate computer physics models so that the models can be refined to provide more reliable predictions about detailed events that occur in nuclear weapon components such as the W88 system. UNICORN represents an advance in test readiness and in gathering equation-of-state data for special nuclear materials.

PTLA: Ensuring Safety through Training

The process for conducting required security training exercises by LANL's protective force is not simple. It requires weeks of planning and incorporates numerous organizations, planning sequences, safety reviews, and precise scenario development.

Following the annually updated Site Safeguards and Security Plan developed by LANL's Security Requirements and Integration Team, the Laboratory's protective force (Day and Zimmermann's Protection Technology Los Alamos [PTLA]), LANL and PTLA special operations experts, and other subject matter experts (SMEs) formulate plausible attack scenarios that could be perpetrated against the Laboratory.

These SMEs, some of whom have combat experience in organizations such as the US Navy's Sea, Air, Land (SEAL) forces and the Army's Delta Force and Ranger battalions, examine the updated plan and plausible attack scenarios using Joint Conflict and Tactical Simulations, a computer modeling program.

Using computer modeling data and SME input, PTLA then initiates numerous small-scale training and validation exercises in preparation for twice-a-year, large-scale exercises. These complex larger events use state-of-the-art laser engagement simulation systems (ESS) to create realistic attack and defense situations that pit PTLA against "adversary" elements in force-on-force encounters.

Detailed Planning

Planning for these large exercises begins approximately 30 working days before the event, beginning with a scoping meeting to prioritize the projected scenarios. The planners coordinate all aspects of scheduling, logistics, safety, facilities, and operational impacts. Then all stakeholders hold a formal planning meeting to finalize an exercise date and establish a detailed timeline. Preliminary and final safety walk-downs of the exercise area, controller training, simulated adversary briefings and rehearsals, evaluator briefing and training needs, development and review of the safety plan and of a hazard identification and mitigation plan (HIMP), and a combined player and controller briefing are all factored into this schedule.

Screening the players. All participants are screened for prohibited items such as live ammunition before they are allowed into a preexercise isolation area. The players are allowed to bring only their uniforms, respirators, and radio earpieces into the area. To prevent weapon-related accidents, each participant forfeits all live ammunition and equipment.

Adversary forces and protective forces are isolated from each other until the exercise begins.





Ready to deploy. Following an annually prepared Site Safeguards and Security Plan, computer-modeled scenarios are selected for potential LANL target locations. The most challenging threat profiles of adversary pathways are used to create attack plans against defense strategies of LANL protection personnel. These large-scale training exercises employ ESS equipment, elite military forces, and state-of-the-art weapons that are modified to prevent injury. Event monitors control all participants from the time they report for duty until the exercise terminates.

In a plan approval meeting conducted 3 days before the exercise, all stakeholders review the exercise plan, HIMP, and safety plan. All senior managers must concur with the entire exercise plan package before it can be executed. Also, to ensure the integrity of the exercise, everyone who participates in the planning phase is required to sign a document that restricts all discussion of dates, times, and locations to personnel who have a strict need to know.

Ensuring the safe completion of such a complex training event requires the planners to identify and evaluate every possible potential hazard, from first assembly of all player groups through their release when the exercise is complete. For example, during development of the HIMP, planners scrutinize potentially hazardous terrain, wildlife that may be in or near the training area, vehicle operations, the likely abilities of the adversary force (e.g., climbing fences or crawling over rough terrain), safety issues regarding the use of weapon and laser (ESS) systems, and problematic weather conditions. After mitigation efforts are developed for each identified hazard, another review is conducted to ensure that all residual safety concerns incur only low health or safety risk but still challenge the skills of the protective force.

Trained event monitors control all participants from the time they report for duty until the exercise is terminated. To prevent accidents, the groups involved (i.e., the adversary force and the protective force) are never allowed to commingle or to be visible to each other. Both groups also are segregated at all times from the shadow force that remains on duty to protect the Laboratory from potential terrorist or other hostile events. This fully armed, fully equipped shadow force is strategically staged in a controlled location for immediate reaction in case of a security-related incident.

Engineered Controls

Numerous engineered controls complement the total safety envelope surrounding the exercises. Although the weapons used in ESS exercises are real, they are heavily modified to prevent the accidental introduction of live ammunition into the exercise area. Dedicated for security training, these weapons cannot function normally. Furthermore, the players use only blank ammunition. Safety experts examine the blanks—cartridge by cartridge—before sealing them in containers that are marked for exercise use only. Individual players inspect the blanks again when their equipment is issued before the exercise.



Equipped for battle. In numerous large-scale exercises each year, PTLA trains its Laboratory protective forces in attack and defense strategies under realistic battle scenarios and conditions. Adversary forces, who are prepared to attack with machine guns, rifles, handguns, rocket launchers, and night-vision goggles, may wear woodland-patterned battle dress uniforms and winter white-over-white camouflage smocks.

As part of the equipment-issue process, a formal methodology directs unscreened players into an issue-area isolation zone where they are processed and screened for prohibited items such as live ammunition. Players are required to deposit all prohibited articles in an amnesty box. The availability of this repository encourages players to surrender prohibited items rather than conceal them in fear of punitive action. All exercise equipment (e.g., belts, holsters, ballistic vests) is issued from a trailer in which dedicated exercise uniforms and equipment are segregated from equipment used for normal duty. The only items the players are allowed to bring into the exercise area are their own individually issued respirators, uniforms, and radio earpieces. Adversary forces wear uniforms that are identical to those of the protective force—a typical adversary method of operation.

The senior exercise controller, in concert with the exercise director, oversees the staging of all player, simulation, adversary-force, and shadow-force elements. The senior controller adheres to an exhaustive checklist to guarantee communications are established, command and control elements are in place, safety issues are addressed, and isolation of the exercise area is complete. At that time, fire, law-enforcement, and emergency medical services are on standby in the immediate area. Only when every check is made and all preparations are in place does the senior exercise controller request permission from the exercise director to initiate the exercise.

During every aspect of the actual force-on-force engagement, trained exercise controllers and evaluators monitor and critique players on an almost one-to-one ratio. Every participant—from the exercise director to the most remote vehicle safety

coordinator—is empowered to announce an exercise freeze if he or she observes a potential safety or security concern. If an exercise freeze is called, all activity halts immediately and may not resume until the concern is resolved. The director may restart or terminate the exercise, contingent on the severity of the concern.




High-tech weaponry. All weapons PTLA uses in its training exercises are heavily modified to prevent the accidental introduction of live ammunition into the exercise area. Fighters and weaponry are equipped with electronic harnesses that record hits from the opposing force. Each hit is entered into a database that is reviewed after the exercise is complete.

When the exercise is complete, the director instructs the senior controller to halt all activity.

The same level of formality adopted during the issue of equipment is applied when the equipment is returned. After all weapons and equipment are accounted for and all players and controllers are out of the exercise area, the shadow force is released to continue its normal duties.

Lessons Learned

A final evaluation of the exercise activity is equally painstaking. PTLA analyzes the effectiveness of all command and control activities, individual and team tactics, response strategies, communications, and the application of simulated deadly force and use of equipment. The controller and evaluator forms completed during the exercise provide valuable information for this final critique.

These hypothetical but plausible scenarios are designed to expose PTLA's forces to worst-case attack events. The result of this training is a flexible, resilient, adaptable force that is prepared to protect the Laboratory. 

Points of contact:

Lloyd Foster, 665-1072, lfoster@lanl.gov

Woody Woodward, 665-7056, woodward@lanl.gov

Waste Reduction at the Laboratory

Trash at Los Alamos National Laboratory is no trifling business.

What began in 1990 as a simple recycling program for office white paper has grown to a list of recyclables that ranges from high-tech materials such as noncontaminated metals to ordinary brush. In 2005, LANL diverted 60% of the Laboratory's rubbish—more than 4000 metric tons (tonnes), or approximately the total weight of 22 Boeing 747 airplanes—from the Los Alamos County landfill into successful recycling projects that involve commercial operations in multiple states.

In 2000, the Laboratory began screening and baling solid sanitary waste (office trash) before disposing of it at the Los Alamos County landfill. In addition, material destined for recycling was also baled at the same facility. Waste Services (WS) Division manages the screening and baling facility, known as the Material Recycling Facility (MRF).

Working in scheduled rotations, technicians pick up recyclables from collection points across the Laboratory and haul the material to the MRF for screening, baling, and/or shipping to recycling distributors.

LANL's expanding recycling program supports efficient use of its resources.

Generator Involvement

Employee involvement and source segregation (users depositing recyclables into different receptacles at the point of collection) are key to a successful recycling program. Having MRF technicians pull recyclables that are not segregated at the point of generation is labor-intensive and adds unnecessary costs to the recycling program. To help minimize avoidable program costs, Laboratory employees are encouraged to segregate their recyclables into roll



Metals collection bins. Employees put waste metals that do not originate in radiological areas into collection bins for recycling. Metals may be delivered to the MRF or collected by the WS recycling staff. Metals are picked up, segregated, and sold for remanufacturing by a contracted local company. As much as possible, generators should segregate more valuable scrap metals (e.g., copper, aluminum, steel, brass) from less valuable metals such as tin.

carts or bins. Cardboard should be flattened and deposited in blue cardboard-recycling dumpsters.

Employees follow similar procedures to recycle uncontaminated metal, tires, wood, plastic, brush, soil, concrete, and asphalt. Additionally, the Laboratory recycles circuit boards, hard drives, oil, food grease, some types of batteries, and light bulbs.

MS A1000

LANL's Mail Stop (MS) A1000 Program recycles colored paper, junk mail, magazines, newspapers, toner cartridges, and viewgraphs. Generators segregate the recyclable material and place it for outgoing mail pickup. When mail staff deliver the mail they collect the A1000 material, taking it to the mailroom for storage and eventual pickup by MRF. This simple system eliminates the need for additional recycling trucks and pickup manpower, thereby reducing fuel and personnel funding resources. The MS A1000 Program won two awards in 2002: a White House Closing the Circle Award and a DOE Pollution Prevention Award.

Environment, Safety, and Security

The MRF operation is crucial to the Laboratory's safety, security, and environmental commitments.

It is critical that waste generators understand what they may put into their trash cans. Prohibited items such as aerosol cans, paint, oils, light bulbs, and batteries may not be placed in the solid sanitary waste stream. The Laboratory has designated waste management coordinators who recycle or dispose of these items properly because EPA's Resource Conservation and Recovery Act (RCRA) requirements exclude those materials from the Los Alamos County landfill. Ignoring RCRA requirements could result in stiff fines for the Laboratory. Because these items could ignite or explode, they also present a safety issue for anyone handling the trash. Additionally, MRF technicians screen the recycle streams for potential security violations such as controlled documents or papers.

Where does it go?

LANL sells all its recyclable fiber material (except wood products) to a material recovery plant that segregates and sells the material to other companies for remanufacturing.

LANL's waste concrete and asphalt are hauled to the county landfill for crushing and reuse. The landfill also accepts brush for composting and soil for reuse as fill material or for cover material at the landfill.



Recycle center. The MRF plans to simplify recycling at the point of segregation by collocating collection bins and posting information about recyclables.

Aluminum cans, aluminum foil, and plastic bottles can be stored in plastic bags next to recycle carts when the carts are full.

Employees should ensure that cans and bottles are completely empty and not contaminated with food or any other waste.

Plastic, aluminum, and white paper are on the same MRF pickup schedule.

LANL's scrap metal recycling program began in the early 1990s and continues to be a major contributor to the success of the Laboratory's recycling program. A local company recycles most of the Laboratory's waste metal, although DOE prohibits recycling metal from radiological areas. In 2005, however, even with this restriction, the Laboratory recycled 1475 tonnes of acceptable metal, including steel, copper, and aluminum.

In 2002, the Laboratory began a wood recycling and reuse program that focused on wood pallets. The program was short-lived due to the difficulty of finding appropriate outlets for the large amount of material collected. In 2005, the Laboratory contracted with a small sawmill in Velarde, New Mexico; the MRF delivers used pallets and scrap wood to the sawmill. The company gives away the scrap wood and rebuilds and resells the pallets.

This program significantly reduced the approximately 200 tonnes of wood waste that would have gone to the Los Alamos County landfill in 2005.

Looking to the Future

The Laboratory continues to monitor its pickup system, including collection point locations, particularly for high-traffic areas and areas known to generate large amounts of recyclable material. Ongoing system improvements will ensure the Laboratory's recycling and waste-reduction practices help sustain efficient use of LANL resources. [NWJ](#)

Points of contact:

Monica Witt, 667-8626, mwitt@lanl.gov

Deba Daymon, 667-9021, deba@lanl.gov



Baled cardboard. LANL bales and recycles approximately 150 tonnes of clean, used, noncontaminated cardboard every year. To prepare for MRF pickup, generators should remove all packing materials and flatten and stack the cardboard. The flattened cardboard should be placed in dedicated blue cardboard-recycling dumpsters, not in or beside trash dumpsters.

Violence in the Workplace



More than 20,000 incidents of workplace violence are reported nationally each year, including verbal threats, unwanted sexual advances, pinching, and pummeling. Often these incidents are paid little notice until someone walks in one morning and “goes postal.”

Americans lament the rampant street crimes across this nation, but are naive about the possibility of violence occurring in our workplaces. Working in a DOE facility among highly educated and motivated people who undergo extensive background checks, meet the requirements of special human reliability programs, and are dedicated to the protection of our country may lead us into the “it can’t happen here” mode of thinking.

Violence can impact any institution for many reasons. Employees’ morale and confidence are eroded by dissatisfied customers, angry citizens who see the institution as an inviting target, crime seeping from the streets into the organization, staff cuts, and efforts to reinvent and reengineer the organization without adding resources. Troubled, marginalized employees are threats to any institution’s well being.

The key to preventing violence at work is understanding that violence is predictable. For example, data from the federal Bureau of Labor Statistics show that workplace violence is most likely to occur on a Monday from 8 A.M. until noon. Violent employees are most frequently men aged 35 to 44 who have been with their employer for 1 to 5 years. These men tend to be loners with multiple professional and personal problems who externalize the reasons for their behavior. They tend to rage, indulge in self-destructive behaviors such as substance abuse or ignoring safety rules, and may have suffered a recent loss of self-esteem at a personal or professional level.

The Los Alamos National Laboratory policy on violence is the same as the policy at all other DOE facilities—zero tolerance. To ensure this policy is effective, all workers must know when violence is most likely to occur and some indicators that could signal trouble.

The key to preventing violence at work is understanding that violence is predictable.

Many situations that occur in the workplace could evoke violent reactions in emotionally marginal employees. Historically, most violent actions occur as a result of or during adverse employment actions, for example, an employee who perceives harassment, high pressure to produce, or autocratic measures imposed by supervisors.

The types of violence that could occur in the workplace are employer directed, domestic related, or property directed. Employer-directed violence is aimed at a symbol of the organization, for example, supervisors, team leaders, or group leaders who the perpetrator equates with the organization. Domestic-related violence can be coworkers in a relationship or a situation that spills into the workplace from home. Property-directed violence can be theft, vandalism, sabotage of equipment, or any other property issue that may be used to “get back” at the organization.

Violence does not happen in the absence of indicators. However, people often do not recognize the indicators of violence or do not voice their concerns until it is too late. Understanding indicators and acting upon them will reduce the frequency, seriousness, and impact of workplace violence.

Research shows that troubled employees tend to have substance abuse problems, histories of mental illness, persistent medical issues, and the inability to cope with high levels of situational stress.

A troubled employee may manifest other indicators, including hyper-vigilance or an unreasonable fear that someone or something is out to get him.

This employee may have an unusual interest in guns, destruction, or weaponry and often shows signs of impaired judgment. According to some researchers, the most important indicator is if an observer feels that something is wrong with a coworker, that observer may be right.

Typical warning signs also include excessive use of alcohol or drugs, compulsive gambling, consistent noncompliant or resistant behavior, extreme mood swings, lack of hygiene, or dressing inappropriately. Other signs to watch for are worker references to previous violent incidents, problems with authority or change, aggressive stances, attitudes, or comments, and religious, ethnic, or political rantings.

Research found that many potentially violent situations are not reported because the troubled employee's actions are taken for granted or employees lack confidence in management's response to a concern, fear reprisals, or are not sure which behaviors indicate potential violence.

What can coworkers, supervisors, and managers do in a potential or suspected violent situation? Employee responsibilities include knowing and abiding by the Laboratory policy, Workplace Violence (AM 732), and notifying management when someone is a victim or knows of violence directed at others.

Managers and supervisors should be fair, communicate their expectations of behavioral issues, listen to the concerns of employees, take appropriate disciplinary action, and think prevention.

An employee who believes immediate action is necessary to respond to violence or a threat of vio-



lence should call 911 and then notify his group- or higher-level manager. Even if the employee believes the threat is not immediate, he or she should notify his group- or higher-level manager. That manager should notify Human Resources Employee Relations, which will coordinate a response, investigate the report, and provide information to managers so that they can take appropriate action.

Nationally, the number of workplace homicides has fallen from more than 1300 in 1994 to approximately 800 in 2004, according to available data from the Bureau of Labor Statistics. But the same government information shows no improvement in nonfatal incidents of workplace violence. The number of assaults has remained relatively unchanged during the same time period.

Like all large organizations, this institution is vulnerable to violence in the workplace. The key to preventing violence is being aware of situations that might result in violence and knowing the behavioral indicators of potentially troubled employees. **NWJ**

Point of contact:

Eric D. Dick, 667-6018, edick@lanl.gov

Safety at LANL: the New Paradigm

Every accident is preventable. That is the conviction of Dick Watkins, Associate Director for Environment, Safety, Health, and Quality (ESH&Q).

Achieving an accident-free Laboratory, however, will require that each person (1) is fully aware of and informed about all hazards associated with his or her environment and (2) understands that safety is a personal—as well as a corporate—responsibility.

Although management can and should provide the regulatory framework and resources needed to accomplish work safely, Watkins believes that only the person doing the work can make regulations or equipment effective because “. . . safety flows from the bottom up, not from the top down”

ISM

Believing strongly that employees are the real drivers in any safety program, Watkins is confident that the Laboratory can avert all accidents if every employee incorporates integrated safety management (ISM) into every aspect of work and every employee is committed to accepting personal responsibility for working safely and to watching out for the safety of coworkers.

The Laboratory moves a step closer to zero accidents and provides a better framework in which to accomplish outstanding science when workers

- define their scope of work,
- identify and analyze all potential hazards before starting work,
- develop controls (i.e., mitigate or eliminate hazards) before initiating a task, and
- provide feedback to peers so that others doing the same work will benefit from their experience.



Dick Watkins, Associate Director for ESH&Q. Watkins is dedicated to achieving a goal of total safety at Los Alamos through employee involvement. Renewing LANL's focus on safety will achieve a mutually beneficial work environment for all LANL employees.

Awareness

Safety awareness is key to safety on the job, Watkins asserts.

Safety is not a standalone thought process that can be isolated from performing work. Although managers must work closely with their staff—whether in a high-risk technical area or in a so-called soft environment such as an office—safety is based on individual participation. An employee who identifies a hazardous situation should stop work and inform his or her manager of the perceived problem so that corrective or mitigative action can be implemented.

Workers who are injured or become ill on the job also should inform their supervisors, who must provide appropriate relief (e.g., arrange for the right tools for the work, ensure appropriate breaks, and if necessary, reassign duties until the injury has healed).

LIR Guidance

In addition, Laboratory Implementation Requirement (LIR) 401-10-01.2 authorizes all Laboratory workers to stop work when they “discover conditions of imminent danger or other hazards” and to communicate those conditions or hazards to other workers who might be at risk.

Attachment A of LIR 401-10-01.2 addresses the approved process for stopping and restarting a worker’s own operations. Attachment B is a flow diagram for stopping or starting another person’s activity or operation.

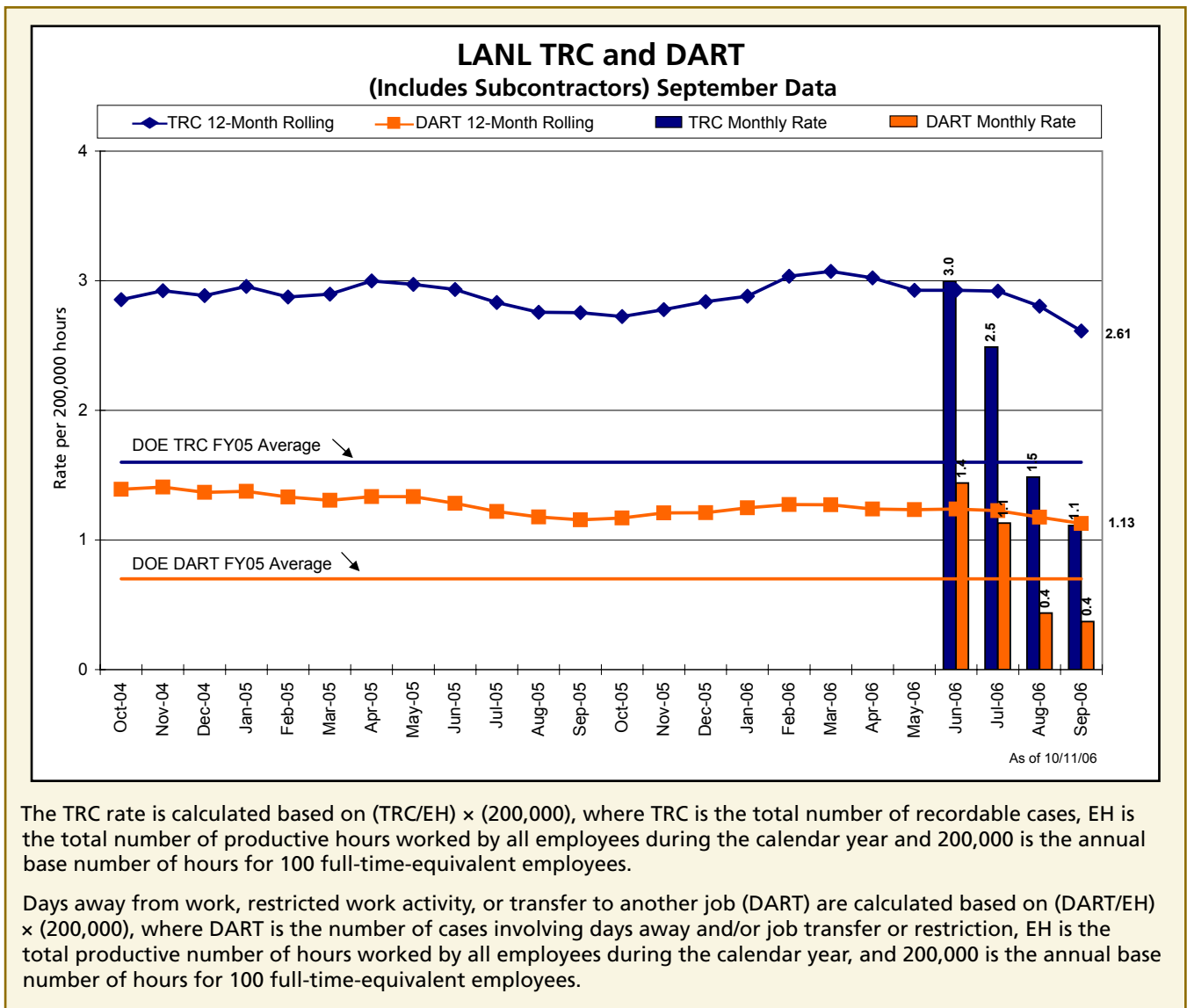
No Risk-Free Environment

Data show that a significant number of industrial

injuries are similar to those that commonly occur in the home, where it’s easy to forget that a familiar, otherwise safe environment is not risk-free. For example, few people notice a coworker balancing on a chair to retrieve an object from a high shelf, a

Employees are the real drivers in every successful safety program.

common—although unsafe—practice at home and elsewhere. However, all Laboratory workers should be aware of the risks associated with this kind of seemingly benign behavior and communicate their unease with such unsafe work practices.




Total Safety

This approach to achieving a goal of total safety at Los Alamos is based on ongoing employee–management cooperation and focusing on prevention.

With increased employee awareness and acceptance of each person’s role in establishing a risk-free workplace and with ISM incorporated into all aspects of Laboratory activity, Watkins believes the Laboratory will become a model for the entire DOE Weapons Complex.

LANL’s new management corporation—Los Alamos National Security (LANS), LLC—backs Watkins in his belief that safety is a cooperative effort between management and individual workers.

In an August memo to Laboratory employees, Director Michael Anastasio stated that “. . . this should be a time to discuss what we, as a laboratory, can do to make safety processes work better and to share best practices and improvements . . .” and that the Laboratory “. . . will take advantage of the LANS parent organizations’ expertise in the area of safety management both in direct and subcontractor work . . .” This renewed focus on safety, he continued, “. . . centers on the principle that we all must be committed to each other’s safety . . .” 

Point of contact:

Dick Watkins, 667-4218, rswatkin@lanl.gov

Is LANL improving?

In June 2006, LANL’s total recordable case (TRC) 12-month rate was approximately 2.93—well above the overall DOE Complex TRC rate of approximately 1.5. By October 2006, the LANL TRC rate decreased by 11% to approximately 2.61.

LANL’s approach to leading and supporting this trend toward total on-the-job safety focuses on the following.

- Improving communication between managers and employees about safety issues and responsibilities

When people are not aware of the safety status of their organization (i.e., how safely their group is working), they tend to become complacent, says Dick Watkins, LANL Associate Director for Environment, Safety, Health, and Quality. However, no one should rely solely on a safety organization for protection, Watkins believes, because “. . . an ESH organization is a support organization, not a control group.”

- Creating a safer work environment through greater employee involvement

Safety is a two-way street that requires individual input at every level of work at the Laboratory.

- Emphasizing the importance of safety awareness across the Laboratory

“Safety is dynamic,” Watkins asserts. “Safety requires continuous revitalization and passion, just as is required for great science.”

A BACKWARD GLANCE

Atomic Annie

After the former Soviet Union conducted its first nuclear test in August 1949, the US reevaluated its postwar defense policies. With the US monopoly on atomic weapons broken, military and political leaders chose to diversify the American stockpile by developing thermonuclear and tactical nuclear weapons. One of the more interesting concepts to come out of this period was atomic artillery, which was successfully tested at the Nevada Proving Grounds (now the Nevada Test Site) in May 1953.

During World War II, the Soviet Union employed hundreds of thousands of soldiers in massive operations designed to bludgeon enemy defensive positions. This emphasis on overwhelming numbers remained a central component of postwar Soviet military strategy. In response, the US developed a reliance on superior technology and firepower, which came to include atomic artillery. A cannon capable of firing an atomic projectile was deemed desirable for several reasons, including pinpoint accuracy that could not be achieved by bombers. Also, deployed artillery afforded field officers the opportunity to respond to enemy attacks as they developed. The cannons could operate during inclement weather and, army leaders argued, in theaters where the enemy had gained air superiority. Such a weapon appeared useful, but many scientists wondered if it was technologically feasible.

Because existing nuclear weapons systems were large and very heavy, the first challenge was to design a warhead that could fit in an artillery shell casing but robust enough to survive the launch environment. To do this, designers chose to scale down a standard gun-type weapon in which one piece of fissionable material is fired down a gun barrel at another piece of fissionable material to initiate a chain reaction.

As work progressed on the nuclear device, the army developed a cannon that could deliver it in combat. The final product, a 280-mm gun weighing nearly 50 tons, could lob atomic rounds as far as 15 miles. The new cannon was nicknamed Atomic Annie.

A field test was scheduled for late spring 1953 as part of the Upshot-Knothole test series. High-ranking government officials, including the Secretary of Defense, two senators, and dozens



Atomic Annie at work during the Upshot-Knothole test series. Four original Atomic Annie guns can still be seen: one each is housed at the National Atomic Museum in Albuquerque, New Mexico; Fort Sill, Oklahoma; Fort Riley, Kansas; and Aberdeen Proving Ground, Maryland.

of congressional representatives, witnessed the test, which was conducted May 25, 1953, at Frenchman Flat, Nevada. The Secretary of the Army observed the event, dubbed Grable, alongside soldiers in trenches 5000 yards from the blast. The device, which obtained a yield of 15 kilotons, traveled 7 miles before detonating approximately 500 feet above the desert floor. Soon after, troops participating in a related military exercise came within 700 meters of ground zero before turning back because of high winds.

Grable was a resounding success. Sterling Cole, Chairman of the Joint Committee on Atomic Energy, stated: “This has been one of the most dramatic demonstrations we have had to date on the enormous advances which have been made in atomic weapons development.” The Grable device, the only cannon-launched atomic artillery shell ever tested by the US, was stockpiled shortly thereafter.

Atomic artillery remained in the US arsenal for decades. Despite the development of improved aircraft and advanced missile systems, the army deployed artillery pieces capable of firing atomic ordnance around the world. Atomic Annie’s descendants added a tactical advantage to the US strategy of deterrence throughout much of the cold war. The US dismantled its last atomic/nuclear artillery shell (W-79) in 2003. [NWU](#)

Point of contact:
Alan Carr, 664-0870, abcarr@lanl.gov